Published in final edited form as:
J Comp Neurol. 2014 December 1; 522(17): 3900–3927. doi:10.1002/cne.23648.

Characterisation of axons expressing the artemin receptor in the female rat urinary bladder: a comparison with other major neuronal populations

Shelley L. Forrest[1], **Peregrine B. Osborne**[1,2], and **Janet R. Keast**[*,1,2]

[1]Pain Management Research Institute and Kolling Institute, University of Sydney at Royal North Shore Hospital, Sydney, NSW, Australia

[2]Department of Anatomy and Neuroscience, University of Melbourne, Melbourne, Victoria, Australia

Abstract

Artemin is a member of the glial cell line-derived neurotrophic factor (GDNF) family that has been strongly implicated in development and regeneration of autonomic nerves, and modulation of nociception. Whereas other members of this family (GDNF and neurturin) primarily target parasympathetic and non-peptidergic sensory neurons, the artemin receptor (GFRα3) is expressed by sympathetic and peptidergic sensory neurons that are also the primary sites of action of nerve growth factor, a powerful modulator of bladder nerves. Many bladder sensory neurons express GFRα3 but it is not known if they represent a specific functional subclass. Therefore, our initial aim was to map the distribution of GFRα3-immunoreactive (-IR) axons in the female rat bladder, using cryostat sections and whole wall thickness preparations. We found that GFRα3-IR axons innervated the detrusor, vasculature and urothelium, but only part of this innervation was sensory. Many noradrenergic sympathetic axons innervating the vasculature were GFRα3-IR, but the noradrenergic innervation of the detrusor was GFRα3-negative. We also identified a prominent source of non-neuronal GFRα3-IR that is likely to be glial. Further characterisation of bladder nerves revealed specific structural features of chemically distinct classes of axon terminals, and a major autonomic source of axons labelled with neurofilament-200, which is commonly used to identify myelinated sensory axons within organs. Intramural neurons were also characterised and quantified. Together, these studies reveal a diverse range of potential targets by which artemin could influence bladder function, nerve regeneration and pain, and provide a strong micro-anatomical framework for understanding bladder physiology and pathophysiology.

Correspondence: Professor Janet R Keast, Department of Anatomy and Neuroscience, University of Melbourne, Vic 3010, Australia, janet.keast@unimelb.edu.au, phone +61 3 8344 5804.
Current addresses: SF: Department of Pathology, University of Sydney, NSW 2006, Australia; JK and PO: Department of Anatomy and Neuroscience, University of Melbourne, Vic 3010, Australia.

Conflict of interest statement: The authors have no conflict of interest relating to this work.

Roles of authors: All authors had full access to all the data in the study and take responsibility for the integrity of the data and the accuracy of data analysis. Study concept and design: SLF, JRK, PBO. Acquisition of data: SLF, JRK. Analysis and interpretation of data: SLF, JRK, PBO. Drafting of article: SLF, JRK, PBO. Critical revision of the article for important intellectual content: SLF, JRK, PBO. Obtained funding: JRK, PBO.

Keywords

urogenital; neurotrophic factor; autonomic; nociception; lower urinary tract; pelvic ganglion

Members of the glial cell line-derived neurotrophic factor (GDNF) family of ligands (GFLs) – GDNF, neurturin and artemin – have numerous functions in the peripheral nervous system (Airaksinen and Saarma, 2002; Bespalov and Saarma, 2007; Ernsberger, 2008). During development, these include regulating the proliferation of neuronal progenitors, neuronal survival, axon guidance and connectivity. Many of these activities are retained in the adult nervous system, where expression of the GFL receptors (GFRs) continues and can be activated to promote axon regeneration. In addition, GFLs have powerful sensitising actions on nociceptors where they have been strongly implicated in inflammatory and neuropathic pain (Elitt et al., 2006; Malin et al., 2006; Tanaka et al., 2011).

An analysis of neuronal classes targeted by the GFLs in the adult peripheral nervous system shows an interesting pattern. First considering the autonomic system, GDNF and neurturin have been most commonly associated with parasympathetic cholinergic neurons (Heuckeroth et al., 1999; Enamoto et al., 2000), in contrast to nerve growth factor (NGF) that targets sympathetic noradrenergic neurons (Glebova and Ginty, 2005; Ernsberger, 2009). GDNF and neurturin also have similar targets in the sensory system. Here, their receptors are expressed by non-peptidergic unmyelinated (C-fiber) neurons, whereas NGF again provides a contrast, targeting peptidergic sensory neurons (Molliver et al., 1995; Bennett et al., 1998; Bennett et al., 2000). These complementary patterns of expression have encouraged the generalisation that GFLs and NGF affect distinct groups of neurons. However, closer inspection of the third GFL member, artemin, shows that this is not the case. Unlike the GDNF and neurturin receptors (GFRα1 and GFRα2), the receptor for artemin, (GFRα3) is not generally expressed by parasympathetic autonomic neurons or non-peptidergic unmyelinated sensory neurons. Instead, it is typically expressed by many of the same neurons that respond to NGF, namely sympathetic neurons and peptidergic unmyelinated sensory neurons. For example, GFRα3 is expressed by almost half of the peptidergic neurons in dorsal root ganglia (DRG) (Bennett et al., 2006; Kalous et al., 2009; Keast et al., 2010), and many sympathetic neurons (Baloh et al., 1998), where it has numerous actions (Andres et al., 2001; Honma et al., 2002). Therefore, in many sympathetic and peptidergic sensory neurons, there is great potential for convergence of signalling from two quite different neurotrophic factor families.

We have recently found that the receptor for artemin, GFRα3, is expressed by almost 40% of unmyelinated bladder-projecting sensory neurons, all of which are peptidergic and express the transducer for nociceptive information, transient receptor potential vanilloid 1 (TRPV1) (Forrest et al., 2013). This raises the question of which tissues within the bladder are potentially influenced by artemin. Moreover, to our knowledge, the expression of GFRα3 in sympathetic axons in the bladder has not been examined. Therefore, our first aim was to define the potential targets for artemin in the bladder using immunohistochemistry for GFRα3 and co-staining with markers of sensory or autonomic neurons. This was performed in cryosections and whole thickness preparations. The latter have not been used

extensively to define the structure of bladder nerves, although they are very informative by allowing structures to be viewed directly rather than inferred from sectional views and facilitating comparisons of larger neuronal fields across different bladder regions (Gabella and Davis, 1998). Therefore, we took this opportunity to describe in detail the distribution and spatial features of major populations of axons in the bladder wall that have primarily or exclusively been described in cryosection studies. As well as providing a reference point for the GFRα3 expression patterns, this enabled us to characterise a small population of intramural ganglion neurons. These neurons are relatively scarce in rats so are rarely found in sections (Iuchi et al., 1994; Alian and Gabella, 1996; Zvarova and Vizzard, 2005).

Materials and Methods

Animals

All procedures were approved by the Animal Care and Ethics Committees of the University of Sydney and Royal North Shore Hospital, as required by the Australian Code of Practice for the Care and Use of Animals for Scientific Purposes (National Health and Medical Research Council of Australia). Twenty-four adult female Sprague Dawley rats (6–10 weeks) were used for these experiments. These comprised ten for diaminobenzidine (DAB)-processed bladder whole mount preparations, two for bladder whole mount preparations processed for immunofluorescence, ninc for bladder cryosections, and three for retrograde tracer injection studies. We performed the study on females in order to form a foundation for future studies focused on cystitis, a condition that in the human population is more common in females and where animal models have been more thoroughly characterised in females. Animals were purchased from the Animal Resources Centre (Murdoch, WA, Australia), and housed under a 12 h light-dark cycle with free access to food and water. Estrous cycle was not monitored or controlled for in these experiments.

Tissue preparation and immunohistochemistry for cryosections

For tissues to be analysed in cryosections, rats were heavily anaesthetised with sodium pentobarbitone (80 mg/kg i.p) and perfused transcardially with 0.9% saline containing 1.25% sodium nitrite and 0.036% heparin, followed by freshly made 4% paraformaldehyde in 0.1 M phosphate buffer (PB, pH 7.4). The urinary bladder and, in some studies, the pelvic ganglia were removed and post-fixed overnight in the same fixative at 4°C, then washed in 0.1M phosphate buffered saline (PBS, pH 7.2) and stored in PBS containing 0.1% sodium azide until sectioning. Tissues were cryoprotected overnight in PBS containing 30% sucrose and cut on a cryostat into 14 μm sections. Bladder sections were cut transversely through the base, into “rings” of sections that included each layer of the bladder wall. Sections were collected onto 0.1% gelatinised slides and distributed between slides so that sections stained for the same substance were sampled at least 42 μm apart. Sections were air-dried, washed in PBS and blocked for 1–2 hours in PBS containing 10% non-immune horse serum and 0.1% triton X-100.

Sections were incubated overnight in combinations of antisera, washed and incubated for 2–3 hours in appropriate host-specific secondaries (Table 1). Each of the primary antibodies has been characterised extensively in previous studies, as summarised in the section on

antibody specificity below. To identify neurons that could potentially be influenced by artemin, we used antibodies raised against its preferred receptor, GFRα3. Other antibodies were chosen on the basis of their known properties and their ability to label particular populations of sensory and autonomic neurons. These were: calcitonin gene-related peptide (CGRP), peptidergic sensory neurons; neuropeptide Y (NPY), sympathetic noradrenergic neurons and the majority of cholinergic bladder-projecting neurons (Mattiasson et al., 1985; Keast and de Groat, 1989); neurofilament 200 kDa (NF200), myelinated sensory neurons (Robertson et al., 1991; Lawson et al., 1993); neuronal nitric oxide synthase (NOS), nitrergic subpopulation of cholinergic autonomic neurons and sensory neurons (Vizzard et al., 1996; Callsen-Cencic and Mense, 1997; Keast, 2006); tyrosine hydroxylase (TH), catecholamine neurons. Markers of non-neuronal cells were also used: S100 and glial fibrillary acidic protein (GFAP), glial cells; smooth muscle actin (SMA), smooth muscle; vimentin (VIM), expressed by interstitial cells.

Antibodies were diluted with 0.1M hypertonic PBS (pH 7.2). All incubations were performed in a humid chamber, in the dark at room temperature. Slides were cover-slipped with carbonate-buffered glycerol (pH 8.6) or, for preparations to be viewed under the confocal microscope, Vectashield mounting medium (Vector Laboratories, Burlingame, CA). Some sections were counter-stained with 4′,6-diamidino-2-phenylindole (DAPI) prior to cover-slipping.

Tissue preparation and immunohistochemistry for whole mounts

In a separate group of rats, the bladder was removed for whole mount preparation. Rats were heavily anaesthetised with sodium pentobarbitone (80 mg/kg i.p.) and perfused transcardially with 350 ml prewash (0.9% saline containing 1.25% sodium nitrite and 0.036% heparin). The bladder was removed and placed in a Petri dish containing prewash. The bladder was bisected longitudinally on the dorsal side, i.e., between the ureters. The bladder was then pinned out flat on a Sylgard-lined Petri dish with the urothelial surface facing upwards and gently stretched to make a circle. The prewash was then replaced with freshly made 4% paraformaldehyde in PB and post-fixed overnight at 4°C. The following day, the pins were removed and bladders washed in PB. The border of the bladder where the pins were inserted was trimmed and the bladders cut into three longitudinal strips (Fig. 1A) before being processed for immunohistochemistry or stored at 4°C in PBS containing 0.05% thimerosol (PBS/thimerosol). Thimerosol was substituted for sodium azide was used to prevent bacterial growth in stored preparations as azide salts can interfere with the DAB reaction that would later be used in processing these tissues.

For non-fluorescent labelling of a single antigen using DAB for visualisation, the protocol followed that described previously (Llewellyn-Smith and Gnanamanickam, 2010). First, bladder strips were washed in PB, then 50% ethanol followed by another wash in 50% ethanol containing 3% H_20_2. All washes were of a large volume (~50 ml) in specimen or glass containers for at least 30 minutes. Strips were then blocked for 30 minutes in PB containing 10% normal horse serum (NHS) before incubation with primary antisera for 5 days at room temperature. Incubations were performed on a shaker at room temperature. Primary antibodies were made up in PB/thimerosol containing 10% non-immune horse

serum, 0.5% triton X-100 and 0.5% thimerosol. Multiwell plates containing 1–2 ml of antibody solution were used for each bladder strip to ensure the antibody had good access to all surfaces of the preparation and to prevent folding.

After three washes in PB, bladder strips were incubated in appropriate biotin-conjugated secondaries made in PB/thimerosol for 5 days at room temperature. Following three washes in PB, bladder strips were incubated in avidin-biotin complex for 5 days at room temperature (6 μl/ml, Vectastain Elite kit; Vector Laboratories, Burlingame CA). Bladder strips were then washed twice in PB followed by an 0.1M acetate buffer pH 6.0 wash before a 20 minute incubation in DAB solution (0.2% D-glucose, 0.04% ammonium chloride, 0.025% diaminobenzidine/100 ml 0.1M acetate buffer pH 6.0, 2% nickel sulfate). A black reaction product was produced by adding glucose oxidase (0.002%) and the reaction stopped by three quick washes with acetate buffer. Bladder strips were washed twice in PB before being mounted onto 0.1% gelatinised slides and air-dried overnight. Strips were then washed twice in H_20 for 15 minutes before being dehydrated in ascending concentrations of ethanol (two 15 minute incubations in 30%, 50%, 70%, 90%, 95% and 100% ethanol) and cleared in histolene (two 15 minute incubations). Bladder strips were coverslipped with DPX water-free mounting media (Crown Scientific, Mulgrave, VIC, Australia) and allowed to dry overnight.

For multi-label immunofluorescence, tissue preparation was as described for the DAB method except PBS was used instead of PB. Following incubation with primary antibody and washes, bladder strips were incubated in appropriate secondary antibodies made up in PBS/thimerosol containing 2% non-immune horse serum and 0.5% triton X-100 for 5 days. Whole mounts were then washed in PBS and mounted onto 0.1% gelatinised slides, coverslipped with Vectashield and sealed with nail polish.

Quantitation of neuronal somata

Immunolabelled somata in DAB-labelled bladder whole mount preparations were counted manually under a 20x objective using a Zeiss Axio Imager M1 microscope (Zeiss Australia, Sydney, Australia). The area of the bladder stained for each substance was calculated using ImageJ/Fiji software (RRID:nif-0000-30467; downloaded from http://fiji.sc/Fiji) and the total number of somata were averaged for each rat and expressed as the mean ± SEM/cm^2. To measure the size of these neuronal somata, images of neurons were captured under a 40x objective and the diameter measured along the major axis using ImagePro Plus (Media Cybernetics, Rockville, MD).

Retrograde tracer studies

To identify bladder-projecting autonomic neurons in the pelvic ganglion, the retrograde tracer Fluorogold (FG; Fluorochrome, Englewood, CO; 4% in sterile saline; total <10 μl) was injected into approximately 8 sites in the urinary bladder base using an insulin syringe with a 30G needle, as described previously (Forrest and Keast, 2008). This was performed under isoflurane anaesthesia (3% for induction, 1.5–2% for maintenance in O_2). These animals were perfused with fixative 7–14 days after surgery (see below) and pelvic ganglia removed for further study in cryosections (14 μm).

Pelvic ganglion sections were immunostained as described above and viewed under an Olympus BX51 Fluorescence microscope. To assess immunoreactivity in bladder-projecting neurons, FG-labelled neurons were classified as NF200-, TH- or NOS-positive and expressed as a percentage of all FG neurons. Under a 40x objective, at least 250 FG neurons were counted from four sections through each ganglion for each rat. To prevent double counting we included only those neurons that were sectioned through the nucleus.

Quantification of axon terminals

Axon terminals in bladder whole mounts were counted on a Zeiss Axio Imager M1 microscope. An axon terminal was defined as the site where a single axon ended in the suburothelial plexus or detrusor. This was determined for GFRα3 and CGRP in the suburothelial plexus and in the detrusor for TH and CGRP, assessing the total number of endings per 500 μm^2. Bladder strips were subdivided into three: base, middle and dome (Fig. 1). Under the 20x objective, a graticule was positioned at the top end of the lower third segment, representing the bladder base. The graticule was used as the grid and moved across the bladder base to make a row. The number of terminals in each area were counted across the bladder in rows and averaged for each rat. Two rows were counted, missing the second row to avoid potentially double counting terminals. The grey squares illustrate the areas of interest (AOI) in which axon terminals were counted (Fig. 1B). The number of CGRP- and GFRα3-IR terminals in the suburothelial plexus in each rat were converted to terminals per mm^2. The same method of counting was used for CGRP- and TH-IR axons in the detrusor. Different types of structures were observed in the TH-IR group so these were categorised into three groups: non-specialised terminals, specialised terminals and those originating from blood vessels. Non-specialised terminals were defined as terminals that did not branch, or branched once before ending; specialised terminals originated from a single axon that issued multiple branches before terminating; and those originating off blood vessels were from para-vascular axons that branched off the vascular tree and then terminated.

Image analysis and figure production

Images of DAB-stained sections were captured with a Zeiss AxioCam MRm camera using Axiovision 4.2 software. Sections processed for immunofluorescence were imaged with an RT Spot camera (Diagnostic Instruments, Sterling Heights, MI) and digitised using Image Pro Plus. For figure production, no adjustments were made to grey-scale images except for minor adjustments to brightness and contrast with the levels command in Adobe Photoshop CS4 (San Jose, CA) to best represent the staining as viewed directly under the microscope. Colorised merged images were produced by pasting grey-scale images into the appropriate colour channel of a 24-bit RGB file created in Photoshop.

In some preparations, immunofluorescence was also visualised with a Leica LCS SP5 II confocal microscope using LAS AF software (Version 2.3.6 build 5381), which was used to acquire images and z-stacks. Excitation wavelengths of 405 nm, 488 nm and 561 nm were used. DAPI (λex = 405 nm) was detected at 420–470 nm. AF488 (λex = 488 nm) was detected at 500–570 nm. Cy3 (λex = 561 nm) was detected at 590–670. All images and z-stacks were acquired using sequential scanning and captured at size 2048 × 2048 pixels with a line average of two to reduce noise. A 1 μm step size was used for z-stacks of the

vasculature and axon bundles, and 0.5 μm step size was used for z-stacks of somata and axons to investigate co-expression. Z-stacks were re-constructed in Photoshop by using the scripts option to load Tif files into an image stack. Images were then converted into smart objects and displayed as the maximum projection. Z-stacks of axon bundles in the detrusor ranged from a thickness of approximately 20–80 μm and comprised 20–80 images (1 μm step size) that were collapsed to form a 2D maximum projection of the z-stack. Z-stacks of the vasculature ranged from a thickness of approximately 30–50 μm and comprised 30–50 collapsed images (1 μm step size); those in the suburothelial plexus were approximately 15 μm thick comprising ~30 collapsed images (0.5 μm step size).

Antibody characterisation

Immunohistochemistry was performed using the primary and secondary antibodies listed in Tables 1 and 2, respectively.

Two antibodies specific for CGRP were used. The goat CGRP polyclonal antibody (RRID:AB_2290729; Batch No. 906) reacts with the whole molecule (1–37) and the 23–37 fragment (C-terminus) but does not cross-react (<0.10%) with calcitonin, somatostatin or amylin 8–37 (dot blot; manufacturer's datasheet). Specific reactivity is eliminated by prior incubation of this antiserum with 10 μM rat CGRP (manufacturer's datasheet) and fluorescence immunostaining of terminals in rat brain is eliminated in an absorption test using 5 μM rat CGRP (Dobolyi et al., 2005). We found a similar pattern of immunoreactivity in DRG and spinal cord as previously described (Chao et al., 2008; Ivanusic, 2009; Kalous et al., 2009).

The rabbit CGRP polyclonal antibody (RRID:AB_2068655; Batch No. LV1529807) reacts with rat CGRP but does not cross-react (<0.01%) with substance P, vasoactive intestinal peptide, neuropeptide Y (porcine), or with human calcitonin, somatostatin or amylin 8–37 (dot blot: manufacturer's datasheet). Specific reactivity of this antibody in frozen sections of rat can be eliminated completely by pre-incubation with 10 μM of rat CGRP (manufacturer's datasheet). This antibody produced a similar pattern of immunoreactivity as previously described (Chao et al., 2008; Ivanusic, 2009; Kalous et al., 2009).

The glial fibrillary acidic protein (GFAP) polyclonal antibody (RRID:AB_10013382; Batch No. 072(102)) cross-reacts with GFAP in cat, dog, mouse, rat, sheep, cow and humans (manufacturer's datasheet). According to the manufacturer's datasheet, in indirect ELISA, this antibody shows no reaction with human plasma and cow serum. This antibody has been documented previously to specifically identify GFAP in glial cells (Cheng et al., 2010; Feig and Haberly, 2011; Vessey et al., 2011).

The GFRα3 polyclonal, affinity purified antibody (RRID:AB_2110295; Batch No. VFU01) in direct ELISA and Western blot detects mouse GFRα3. In direct ELISA, this antibody shows approximately 10% cross-reactivity with recombinant human GFRα3 and less than 2% cross-reactivity with recombinant mouse GFRα2, recombinant mouse GFRα4 and recombinant rat GFRα1 (manufacturer's datasheet). This antibody produced a similar pattern of immunoreactivity in DRGs as previously described using the same antibody (Elitt et al., 2006; Malin et al., 2006) or another GFRα3 antibody that has also been demonstrated

as specific using Western blotting and ELISA (Orozco et al., 2001). Further, the pattern of staining in DRG that we have previously demonstrated with this antibody closely matches the results of in situ hybridisation studies on DRG (Bennett et al., 2000; Bennett et al., 2006).

The neurofilament 200 (NF200, clone N52) monoclonal antibody (RRID:AB_477257; Batch No. 017K4802) was raised from a hybridoma produced by the fusion of mouse myeloma cells and splenocytes from an immunised mouse. In Western blot this antibody specifically localises the neurofilament of molecular weight 200 kDa in rat spinal cord using an immunoblotting technique and does not cross-react with other intermediate filament proteins. According to the manufacturer's datasheet, this antibody shows broad species cross-reactivity by recognising neurofilament in the central and peripheral nervous system in human, monkey, pig, rabbit, hamster, rat and mouse. We found a similar pattern of immunoreactivity using this antibody in DRG as previously described (Robertson et al., 1991; Zylka et al., 2005; Scherrer et al., 2010).

The neuropeptide Y (NPY) polyclonal antibody (RRID:AB_572253; Batch No. 208001) reacts with NPY in a range of species including rat, cat and human. All immunostaining signal is abolished by preabsorbed by NPY but unaffected by pre-incubation with peptide YY, avian pancreatic polypeptide, vasoactive intestinal peptide, somatostatin and cholecystokinin (manufacturer's datasheet). This antibody produces no staining in the forebrain or brainstem of an NPY knockout mouse (Lee et al., 2013). This antibody produced a similar pattern of staining in the bladder as previous publications (Mattiasson et al., 1985; Iuchi et al., 1994).

The neuronal nitric oxide synthase (NOS) polyclonal antibody (RRID:AB_2313734; Batch No. 441121A) reacts with ~160 kDa nNOS and does not cross-react with related eNOS or iNOS proteins. This antibody reacts with a ~160 kDa band on Western blot of rat and mouse tissue lysates (manufacturer's datasheet). This antibody produced a similar pattern of immunoreactivity in rat DRG and bladder as previously described (Vizzard et al., 1996; Forrest et al., 2013).

The anti-S100 monoclonal antibody (RRID:AB_571112; Batch No. 18070419) reacts with intact alpha and beta subunits of bovine, human and murine S100 protein as determined by immunoprecipitation profiles and Western blotting detects a single expected banded in PC12 lysates (manufacturer's datasheet). This antibody has previously been demonstrated to specifically label glial cells (Chao et al., 2008).

The smooth muscle actin-α (SMA) monoclonal antibody (RRID:AB_262054) is derived from the 1A4 hybridoma produced by the fusion of mouse myeloma cells and splenocytes from mice immunised with the NH_2 terminal synthetic decapeptide of α-smooth muscle actin, coupled to keyhole limpet hemocyanin (manufacturer's datasheet). This antibody is specific to the α-actin single isoform as determined by immunoblotting on SDS PAGE, ELISA and 2D-PAGE (Skalli et al., 1986) and cross-reacts with human, rabbit, rat, mouse, bovine, frog, goat, guinea pig, dog, sheep, snake and chicken (manufacturer's datasheet).

This antibody produced a similar pattern of immunoreactivity as described previously (Faggian et al., 1998; Goldshmit et al., 2006).

The tyrosine hydroxylase (TH) polyclonal antibody (RRID:AB_477627; Batch No. NG1830749) cross-reacts with most mammalian and many non-mammalian species including rat, mouse, ferret and Aplysia (manufacturer's datasheet). In Western blot this antibody specifically labels a single band at approximately 62 kDa (manufacturer's datasheet). In the bladder, this antibody produced a similar pattern of immunoreactivity as reported previously (Wakabayashi et al., 1994; Llewellyn-Smith and Gnanamanickam, 2010).

The vimentin (Vim) monoclonal antibody (RRID:AB_477627; Batch No. 090M4817) cross reacts with a variety of species including human, pig, chicken and rat; Western blotting identifies a band at ~58 kDa, as appropriate (manufacturer's datasheet). This antibody produced a similar pattern of immunoreactivity as previously described (Davidson and McCloskey, 2005; Grol et al., 2008).

Results

Distribution of GFRα3-IR in relation to peptidergic afferent distribution

We have previously demonstrated that approximately 30% of bladder-projecting afferent neurons are GFRα3-immunoreactive (IR) and almost all of these were found in the peptidergic CGRP-IR population, of which they comprised approximately half (Forrest et al., 2013). Therefore, we predicted that CGRP-IR axons in the bladder would be more prevalent than GFRα3-IR axons. The distribution of CGRP-IR axons throughout the bladder was similar to a previous report of whole mount labelling (Gabella and Davis, 1998). There were three main targets: the detrusor, suburothelial plexus and vasculature, each of which will be described in more detail below.

Detrusor—CGRP-IR axons were prevalent in the detrusor and did not appear to differ in density between each bladder region (Fig. 2A–C), where they were present in axon bundles that traversed the bladder or as single, varicose axons (Fig. 2A–C, G, H). CGRP-IR terminals occurred throughout the whole thickness of the detrusor, and were unspecialised simple endings of single fibers or single fibers with one branch point (Fig. 2I, J). Quantification of whole thickness preparations revealed 139 ± 12 CGRP-IR terminals/mm^2 (n=4) in the detrusor of the bladder base. Many CGRP-IR axons also travelled in para-vascular axons throughout the detrusor. These will be described in more detail below in the section focused on vasculature. Neither neuronal nor non-neuronal CGRP-IR cells were observed in the detrusor.

GFRα3-IR axons were also prevalent in the detrusor, and like CGRP-IR axons, were distributed evenly throughout the bladder (Fig. 2D–F). These were present in bundles of multiple axons that ran parallel to the muscle fibers or as single, varicose axons with unspecialised endings (Fig. 2K–N). GFRα3-IR axons innervated the whole thickness of the detrusor but were preferentially located on the serosal aspect. GFRα3-IR terminals were not quantified as their labelling intensity was quite variable and regions of termination could not

always be identified. In addition to GFRα3-IR axons, many small GFRα3-IR cells were embedded in the detrusor of each bladder region (Fig. 2O–S). The majority of these were elongated cells with processes. They were always closely associated with single axons or bundles of axons and were present in higher density close to the serosal surface. These GFRα3-IR structures were much smaller than neurons, did not demonstrate the presence of a process sufficiently elongated to be considered a potential axon and were much too prevalent to be regarded as neurons (given the scarcity of neurons in rat bladder (Iuchi et al., 1994; Alian and Gabella, 1996; Zvarova and Vizzard, 2005)). Therefore we considered that they were non-neuronal cells and for brevity have referred to them as such. Their further characterisation is described below. Many GFRα3-IR axons were closely associated with blood vessels and will be described in more detail below in a section focused on vasculature.

Co-expression studies were then performed to directly determine if GFRα3-IR was expressed in peptidergic afferent axons in the detrusor (Fig. 3). While there was a significant degree of co-expression, many axons were immunoreactive for only one or other of the markers (Fig. 3A–F). Because all GFRα3-IR bladder sensory neurons express CGRP-IR (Forrest et al., 2013), this indicates that some GFRα3-IRaxons in the detrusor are not sensory. This is explored further below. GFRα3-IR non-neuronal cells with elongated processes were not immunoreactive for CGRP, although many of these cells were closely associated with CGRP-IR axons (Fig. 3G–J).

Suburothelial plexus—As previously described (Gabella and Davis, 1998), CGRP-IR axons were present near and within the urothelium, and were more prevalent in the bladder base than the middle and dome (Fig. 4A–C). These axons formed a dense network and are referred to as the suburothelial plexus. GFRα3-IR axons were also prevalent in the suburothelial plexus and most dense in the bladder base, progressively decreasing towards the bladder dome (Fig. 4D–F). In addition to unspecialised endings, two types of CGRP-IR closed axonal loops were observed in the suburothelial plexus. Here, a single axon branched into two and appeared to re-join, forming a loop in the middle of an axon (Fig. 4G), or a loop formed at the end of a termination (Fig. 4H, i). Both types of closed axonal loops were also associated with GFRα3-IR axons in the suburothelial plexus (Fig. 4J, K). Like CGRP, these loops were not present in the detrusor.

CGRP-IR axons in the suburothelial plexus were typically varicose and terminal endings were easily visualised (Fig. 4M–O). GFRα3-IR varicose endings also were present in the suburothelial plexus and more readily visible than those in the detrusor. They were not as common as CGRP-IR endings (GFRα3: 31 ± 1/mm^2 vs. CGRP: 70 ± 4/mm^2). Like CGRP-IR axons at this site, they terminated with a varicosity (Fig. 4P–R). Double-labeling fluorescence demonstrated directly that almost all GFRα3-IR axons in the suburothelial plexus were CGRP-positive, but that many CGRP-IR axons were GFRα3-negative (Fig. 3K–P).

Many GFRα3-IR non-neuronal cells were present throughout the suburothelial plexus. These were small cells with processes that branched to closely appose GFRα3-IR axons (Fig. 4J–L). They had a similar appearance to those in the detrusor. As in the detrusor, the

small GFRα3-IR non-neuronal cells in the suburothelial plexus were not immunoreactive for CGRP but were occasionally in close proximity to CGRP-IR axons.

Vasculature—Both CGRP- and GFRα3-IR axons were associated with the vasculature in the lamina propria and traversing the detrusor (Fig. 5). The majority of CGRP-IR nerves associated with the vasculature were small bundles of para-vascular axons. These were found on primary, secondary and tertiary branches of the vascular tree (Fig. 5A–C). CGRP-IR para-vascular axons were rarely found on quaternary vessels. The primary vessels also contained some CGRP-IR peri-vascular axons (Fig. 5A, B) that branched to form a sparse meshwork around the vessel. CGRP-IR peri-vascular axons were relatively sparse on all other branches of the vascular tree (Fig. 5B, C).

Numerous GFRα3-IR axons were associated with the vascular tree and consisted of both para- and peri-vascular axons (Fig. 5D–F). GFRα3-IR para-vascular axons travelled in small bundles and in contrast to CGRP were found on all branches of the vascular tree. Peri-vascular GFRα3-IR axons were associated with both primary and secondary vessels, were less prevalent on proximal aspects of tertiary vessels and did not extend to distal tertiary or quaternary vessels.

Double labeling clearly demonstrated that in the vasculature GFRα3-IR axons were more prevalent than CGRP-IR axons, indicating that some GFRα3-IR axons associated with the vasculature were not peptidergic afferent axons. This was confirmed by double labeling, which showed many GFRα3-IR paravascular axons and the majority of GFRα3-IR perivascular axons were CGRP-negative (Fig. 5G–O). Therefore, the axons that extend furthest down the vascular tree and likely to directly innervate the vascular muscle are a non-afferent population of GFRα3-IR axons. At all levels of the vascular tree, small GFRα3-IR non-neuronal cells were closely associated with axons (not shown).

GFRα3-IR noradrenergic axons

Because the majority of peri-vascular GFRα3-IR axons were not immunoreactive for CGRP, we considered that GFRα3-IR could be expressed in sympathetic vasoconstrictor axons. These have been well documented (Gibbins, 1992) and can be visualised using TH. The following section summarises the expression of GFRα3-IR relative to the two primary populations of sympathetic axons in the bladder, vasoconstrictor axons and axons innervating the detrusor of the bladder base.

Vasculature—TH-IR axons densely innervated the vascular tree of the detrusor and lamina propria (Fig. 6A–C). They consisted of both para- and peri-vascular axons and extended along most of the vascular tree but rarely to the most distal (quaternary) branches. Both components of the noradrenergic innervation decreased in density with branching of the vessels. Double-labeling showed that co-expression of TH- and CGRP-IR did not occur in para- or peri-vascular axons (Fig. 6D–I). TH-IR para- and peri-vascular axons were more prevalent than peptidergic afferent axons (Fig 6D–I), and TH-IR axons extended further along the vascular tree (Fig. 6D–F). Double-labeling also showed that many of the para- and perivascular GFRα3-IR axons were TH-IR but that not all TH-IR axons were GFRα3-IR (Fig. 6J–O). In summary, GFRα3-IR axons associated with the bladder vasculature were of

two types: peptidergic afferent and sympathetic noradrenergic. The latter extended further along the vascular tree.

Detrusor—In addition to the vasculature, sympathetic axons also innervate the detrusor (Wakabayashi et al., 1993; Wakabayashi et al., 1994; Warburton and Santer, 1994), therefore we investigated if GFRα3-IR was expressed in this population of noradrenergic axons. In contrast to the dense noradrenergic innervation of the vasculature, TH-IR axons were sparse in the detrusor and primarily confined to the bladder base (Fig. 7A–F). The majority of TH-IR axons in the detrusor were present in bundles consisting of multiple non-varicose axons or single varicose axons (Fig. 7A–F). Quantification in full thickness detrusor confirmed that these were much less prevalent than peptidergic afferent terminals (40 ± 7 TH-IR axon terminals/mm^2; n = 4). TH-IR terminals consisted of 3 structural types: “non-specialised” (i.e. single fiber endings or a branch into two terminals) (Fig. 7D), “specialised” (multiple branches) (Fig. 7E) and terminals that branched off from para-vascular axons (Fig. 7F). Both non-specialised and specialised endings were present throughout the whole thickness of the detrusor, whereas endings originating from para-vascular axons were most common in the lamina propria where they emanated from distal branches of vascular trees. TH-IR axons were not present in the suburothelial plexus and TH-IR intramural neurons were rarely identified in the detrusor. Double labeling showed that in the detrusor, although some TH-IR axons were in close proximity to GFRα3-IR axons, their immunoreactivity rarely co-localised (Fig. 7G–L).

GFRα3-IR in non-neuronal cells

The presence of GFRα3-IR in non-neuronal cells was unexpected so we conducted an additional group of co-labelling studies to identify their cell type. Myofibroblasts and interstitial cells express vimentin (Vim) (Davidson and McCloskey, 2005; McCloskey, 2010). Vim-IR cells and their processes were prevalent in the detrusor, vasculature and forming a dense band beneath the urothelium (Fig. 8A–D). Co-expression of GFRα3-IR with Vim-IR was rare or absent in each of these tissues (Fig. 8E–P). Immunolabelling for smooth muscle actin (SMA) showed a broad distribution (Fig. 8Q–T) but failed to show co-expression with GFRα3 (Fig. 8U-BB).

Glial fibrillary acidic protein (GFAP) was used to identify glial cells associated with axons in the bladder. GFAP-IR structures resembling glial cells or their processes were located in most tissues (Fig. 9A–C) and were closely associated with individual axons and bundles of axons. In the detrusor, these were more common towards the serosal aspect (especially within the larger bundles of axons); they were also found with the vasculature and in the lamina propria. Further inspection of the dense band of GFAP-IR beneath the urothelium did not resemble glial cells, but was not characterised further. We found that there was only partial co-expression between GFAP and GFRα3-IR (Fig. 9H–S), indicating that at least some of the GFRα3-IR cells were glia. The majority of GFRα3-IR cells associated with vasculature were GFAP-IR. Similar analyses were performed with S100, an alternative marker of glial cells in the bladder. This showed a comparable pattern of staining within the bladder tissues, but without the dense band of labelling under the urothelium seen with

GFAP. As with GFAP, GFRα3-IR showed only partial co-expression with S100 (Fig. 9T–W).

Other neuronal markers

We included in our study three other neuronal markers that are frequently associated with peripheral neural function. First, we studied neurofilament-200 (NF200) that we predicted would identify myelinated afferents (Robertson et al., 1991; Scherrer et al., 2010). Second, we investigated neuropeptide Y (NPY), which is expressed by the majority of parasympathetic axons in the rat bladder (Mattiasson et al., 1985; Keast and de Groat, 1989); NPY is also expressed in sympathetic vasoconstrictor axons (see above). Third, we mapped neuronal nitric oxide synthase (NOS), which is expressed by a subgroup of parasympathetic bladder axons (Keast and de Groat, 1989; Ding et al., 1993; Alm et al., 1995a; Alm et al., 1995b) and some of the sensory axons (Vizzard et al., 1996; Callsen-Cencic and Mense, 1997). As well as providing additional comparators for the GFRα3-IR labelling, this set of studies also allowed us to visualise many of the neuronal cell bodies associated with the bladder wall.

NF200—NF200-IR is found in medium-large diameter, myelinated sensory neurons (Robertson et al., 1991; Scherrer et al., 2010). Although many bladder sensory neurons are lightly myelinated and express NF200 (Hayashi et al., 2009; Russo et al., 2013), GFRα3-IR is expressed by unmyelinated neurons (Forrest et al., 2013) so was predicted to be in a separate population of bladder axons.

NF200-IR axons were prevalent in the detrusor, where larger bundles of positively stained axons were more common in the base of the bladder (Fig. 10A–C). The majority of NF200-IR axons travelled in large axon bundles; very few NF200-IR single axons were observed (Fig. 10D–F). NF200-IR axons were typically non-varicose and their terminals were sparse and difficult to visualise. Few NF200-IR axons were associated with the vasculature; these consisted of para-vascular axons on primary and secondary branches of the vascular tree (Fig. 10G–I). NF200-IR para-vascular axons rarely branched or were observed past the secondary vessels. Double labeling showed that almost all large bundles of NF200-IR axons had no immunoreactivity for GFRα3 (Fig. 10M–O), however co-expression was observed in some single NF200-IR axons (Fig. 10P–R).

NF200-IR intramural neurons (diameter 15.2 ± 0.6 μm) were closely associated with single axons or axon bundles in the detrusor (Fig. 10J–L). NF200-IR neurons were evenly distributed throughout the bladder (22 ± 4 neurons/cm^2, n= 4). Many had short processes and were found individually or in small clusters containing 3–4 neurons. The presence of these NF200-IR somata raised the possibility that NF200-IR may be expressed in autonomic axons originating from pelvic ganglia (PG). To investigate this possibility, we examined the distribution of NF200-IR in the PG, focusing on neurons retrogradely labelled from the bladder (Fig. 11).

NF200-IR neurons and axons were prevalent in the PG (Fig. 11A, E, I, M). We found that 22.4 ± 0.8% of bladder-projecting PG neurons immunostain for NOS, <2% immunostain for TH and 82.1 ± 1.9% immunostain for NF200 (Fig. 11E–P). Double labeling of the bladder-

projecting neurons showed that 92.0 ± 3.4% of the NOS-IR bladder neurons immunostain for NF200 (Fig. 11E–H). Although a very small percentage of FG neurons in the female rat PG were immunoreactive for TH, they were all immunoreactive for NF200-IR. This is the first time NF200-IR has been demonstrated in the PG and suggests that NF200 is expressed by both afferent and autonomic post-ganglionic axons in the bladder, the majority of which were cholinergic.

NPY—The detrusor was densely innervated by NPY-IR axons. These were present as bundles and numerous single varicose axons that did not change significantly in density between the base and dome (Fig. 12A–C). Apart from non-specialised endings, it was difficult to identify other types of terminal structures due to the heavy density of axons. NPY-IR somata (diameter 16.0 ± 0.6 μm) were present in the detrusor, evenly distributed throughout the bladder (14 ± 7 neurons/cm^2; n = 4). They were found alone or in clusters, associated with axon bundles or attached to single axons (Fig. 12D–F).

NPY-IR axons were associated with the vasculature in the lamina propria and traversing the detrusor. These consisted of both para- and peri-vascular axons that densely innervated all branches of the vascular tree (Fig. 12G–I). Peri-vascular axons formed a dense meshwork on primary and secondary vessels but were less dense on distal vessels. NPY-IR axons were also associated with the suburothelial plexus. These were more prevalent in the bladder base and became progressively less dense towards the bladder dome (Fig. 12J–L). All NPY-IR axons in the suburothelial plexus were varicose, the majority branching from para-vascular axon bundles (Fig. 12M–O).

NOS—NOS-IR axons were less common than NPY axons in the detrusor. Their density did not vary in the detrusor of different bladder regions (Fig. 13A–C). All NOS-IR axons were varicose and travelled as single axons or in axon bundles that traversed the bladder. Specialised nerve endings (multiple branch points arising from a single axon) were common in NOS-IR axons of the detrusor (Fig. 13D–F). NOS-IR axons were also associated with the vasculature in the detrusor (Fig. 13G, H) and lamina propria (Fig. 13I). The majority of these NOS-IR axons were para-vascular, with relatively few peri-vascular axons. Some NOS-IR endings were observed in the suburothelial plexus, originating from para-vascular axons branching off the vascular tree (Fig. 13I).

NOS-IR neurons (diameter 14.6 ± 0.9 μm) were present in the detrusor and were evenly distributed throughout the bladder (8 ± 1 neurons/cm^2; n = 5) (Fig. 13J–L). They were closely associated with axon bundles or attached to single axons and found singly or clusters of up to six somata. The length of their dendrites varied considerably between neurons and some had no dendrites.

NOS-IR axons were also present beneath the urothelium, where they were more prevalent in the bladder base than the middle and dome of the bladder (Fig. 13M–O). Almost all NOS-IR axons in the suburothelial plexus were varicose. NOS-IR closed axonal loops originating from the middle of axons were also present (Fig. 13P), although closed axonal loops at axon terminals (as seen for CGRP) were not observed. NOS-IR terminals in the suburothelial plexus either did not branch, or branched into only two before terminating (Fig. 13Q, R).

Some of these originated from para-vascular axons. Moderate to weak labelling of urothelial cells was also evident (Fig. 13M–R).

Discussion

This study identified numerous potential targets within the bladder wall for the neurotrophic factor, artemin. These included a major subpopulation of peptidergic afferent axons within the detrusor, vasculature and suburothelial plexus, many sympathetic vasoconstrictor axons and a population of non-neuronal cells that include glia. Artemin is unlikely to directly influence parasympathetic axons or sympathetic axons innervating the detrusor. Together, this provides for a wide range of potential actions on sensory or autonomic function. By utilising whole wall thickness preparations, the study also revealed new structural features of subpopulations of sensory and autonomic nerves in the bladder. Finally, NF200 is commonly used as a marker of myelinated afferents but we found it is also heavily expressed by the majority of pelvic autonomic ganglion cells, including most bladder-projecting neurons. Together, these new findings provide a strong micro-anatomical framework for studies of bladder physiology and pathophysiology.

Potential targets and actions of artemin in the bladder

Artemin has diverse actions on peripheral nerves, including pro-generative effects and modulating nociception (Elitt et al., 2006; Malin et al., 2006; Wang et al., 2011; Wang et al., 2014). While there is still debate regarding its categorisation as ‘nociceptive’ or ‘anti-nociceptive’, the strong potential for influence on bladder afferent neurons is indicated by expression of its preferred receptor, GFRα3, in around 40% of the population; all of this population express the nociceptive transducer, TRPV1 (Forrest et al., 2013). Moreover, expression of GFRα3 by many sympathetic neurons innervating the bladder vasculature provides another potential mechanism for artemin to influence bladder function. The current drive to develop small molecule ligands of GFRs to influence neural regeneration or pain (Gardell et al., 2003; Wang et al., 2008) may also benefit studies of bladder nerve repair after pelvic surgery or development of visceral pain.

Understanding the function of endogenous artemin is a priority, but to our knowledge the source of artemin in the bladder and other pelvic organs has not been investigated. In the vasculature, smooth muscle cells express artemin and noradrenergic axons express GFRα3-IR (Honma et al., 2002), but neither have been specifically investigated in the bladder. In contrast, NGF, GDNF and neurturin are all known to be synthesised by the bladder and other pelvic organs (Kawakami et al., 2003; Leon et al., 1994; Vizzard, 2000; Widenfalk et al., 1997; Widenfalk et al., 2000). Schwann cells can also produce GDNF, providing neurotrophic support for injured axons (Springer et al., 1994; Trupp et al., 1997; Zhang et al., 2009). Both NGF and GDNF levels in the bladder are increased following bladder inflammation and spinal cord injury (Vizzard, 2000), suggesting a potential mechanism of increased excitability and altered neurochemical properties of bladder afferent neurons. Artemin should also be investigated in these situations.

Signalling by artemin requires GFRα3 and the receptor tyrosine kinase, RET (rearranged during transfection) (Airaksinen and Saarma, 2002), so our results need to take into account

the presence and distribution of RET in the bladder. Almost all GFRα3-IR DRG neurons co-express RET (Orozco et al., 2001), but we do not know if RET is transported peripherally within GFRα3-IR bladder axons or expressed by the GFRα3-IR non-neuronal cells. An immunohistochemical study by Yang and colleagues reported the presence of GFRα3- and RET-IR axons in the rat bladder, however the signal was described as weak and the data was not shown (Yang et al., 2006). These authors also reported occasional RET-IR intramural neurons in the bladder. We did not investigate RET localisation in the bladder wall because we were unable to develop immunolabelling of sufficient quality, however this would be an important question to pursue with *in situ* hybridisation or reporter mice.

The first part of our study explored the potential for artemin to target peptidergic afferent axons in different regions and tissues of the bladder. CGRP-IR axons were evenly distributed throughout the detrusor but were far less prevalent than autonomic axons labelled with NPY. As previously reported (Yokokawa et al., 1986; Gabella and Davis, 1998), CGRP-IR axons had three main targets in the bladder: detrusor, suburothelial plexus and the vasculature. We demonstrated that GFRα3-IR axons were prevalent and had similar targets as CGRP-IR axons but were only expressed in a subgroup of these axons. This is consistent with our recent retrograde labeling study, which showed that all of the GFRα3-IR bladder sensory neurons expressed CGRP, but only about half of the CGRP-IR bladder sensory neurons expressed GFRα3-IR (Forrest et al., 2013). This study also showed that >90% of the GFRα3-IR and CGRP-IR bladder neurons expressed the nociceptive transducer, TRPV1. Therefore, we would predict that sensory neurons in each of the bladder tissues innervated by CGRP-IR axons have a nociceptive role. Further, experimental destruction of TRPV1-expressing axons within the bladder (e.g., by capsaicin treatment) would be predicted to have widespread actions on peptidergic (and some non-peptidergic) axons. We did not include TRPV1 immunostaining in this study because we have been unable to obtain consistent and convincing labelling of axons within the bladder wall.

We also showed that GFRα3-IR is expressed by many noradrenergic vasoconstrictor peri-vascular axons in the bladder but not by noradrenergic nerves innervating the detrusor. Artemin promotes the survival of sympathetic neurons (Baloh et al., 1998) and is required for sympathetic axons to reach their target organs during development (Honma et al., 2002). Sympathetic neurons that innervate the vasculature elsewhere have also been found to express GFRα3 and RET (Damon et al., 2007). Our observation that GFRα3 is expressed by both sensory and sympathetic axons innervating blood vessels raises the possibility that vascular-derived artemin (Honma et al., 2002; McIlvried et al., 2010) is an important guidance factor for both sympathetic and peptidergic sensory axons. We found no evidence of GFRα3-IR expression in vascular smooth muscle cells although GFRα3 mRNA and protein have been reported in smooth muscle cells of neonatal arteries (Damon et al., 2007). It is possible that artemin is down-regulated in these cells postnatally once sympathetic axons have already reached their target, that it does not occur in the bladder or that our immunohistochemical technique was insufficient to detect this expression.

In addition to these two distinct neuronal expression sites (sensory and sympathetic), we found evidence for a non-neuronal source of GFRα3 in the bladder. Our observations of only partial co-expression with glial markers (S100, GFAP) suggests an additional source,

however the size and shape of GFRα3-IR cells, and lack of vimentin expression, most closely resembles a glial phenotype. Alternatively, it is possible that our glial markers did not stain the entire population of glial cells. Irrespective, it is clear that many glial cells do not express GFRα3, indicating the presence of two distinct glial populations. The actions of artemin on peripheral glia have not been determined but may relate to regenerative mechanisms.

Structural features of bladder innervation

By exploiting whole thickness bladder preparations, we were able to identify a number of features of bladder innervation that have not been reported previously, and to provide additional perspectives on earlier observations. However, a limitation of our study is that we did not separately differentiate or analyse innervation of the trigone or the points at which the ureters enter the bladder.

A number of structures were found near the points of axon termination, and these appeared to differ between chemical classes of axons and tissues (detrusor vs. suburothelial plexus). For example, complex endings were only observed for TH- and NOS-IR axons in the detrusor, and closed axonal loops were only found in the suburothelial plexus. The functional significance of these structural differences is not known but could potentially be correlated in functional studies of bladder sensory function that incorporate both terminal visualisation and physiological characterisation (Zagorodnyuk et al., 2009; Zagorodnyuk et al., 2010). Whereas the majority of antibodies used in this study were specific markers of either sensory or autonomic nerve populations, interpretation of NOS immunolabelling is more complex because it has both a sensory and parasympathetic source (Vizzard et al., 1996; Callsen-Cencic and Mense, 1997; Keast, 2006).

Axons immunolabelled for the structural protein, NF200, were included in the study in order to map myelinated axons within the bladder wall, as NF200 is characteristic of these neuronal cell bodies in DRG (Lawson et al., 1993; Forrest et al., 2013). However, a limitation of this component of the study was that NF200 incompletely labelled the axon, rarely allowing visualisation of its termination point. Of greater interest, we found that NF200 axons had a second site of origin – autonomic neurons in the pelvic ganglion. This is consistent with reports of NF200-IR in sympathetic and enteric ganglia (Trojanowski et al., 1986; Chiocchetti et al., 2009). While the functional implication of this expression is not known, it is critical to bear this source in mind when viewing NF200-IR axons within experimental or pathological samples.

Intramural bladder neurons were originally regarded as absent in rats (Gabella, 1990) but more recent studies have demonstrated that they are present (Iuchi et al., 1994; Alian and Gabella, 1996; Zvarova and Vizzard, 2005), albeit sparse compared to other species (el-Badawi and Schenk, 1966; Dixon et al., 1983; Gabella, 1990; Smet et al., 1996; Zhou and Ling, 1998). By using whole thickness preparations, we were able to quantify and characterise these neurons associated with the detrusor that were labelled by antibodies against NF200, NOS and NPY. We did not perform co-expression studies to determine if these represent three separate or overlapping populations. NF200-IR intramural neurons have been reported in the cat, almost all of which were found to be intramural

parasympathetic ganglion neurons and contained choline acetyltransferase (Ruan et al., 2006). NF200-IR intramural neurons have also been reported in the guinea pig (Coelho et al., 2012). In rats, intramural neurons are more prevalent early in life, but appear to decrease during the postnatal period (Zvarova and Vizzard, 2005). We propose that they provide a minor component of the motor innervation of the detrusor. Afferent axon terminals are also reported to make contact with intramural ganglia (Smet et al., 1996; Zhou and Ling, 1998) but CGRP and other markers of afferent neurons are not expressed by intramural neurons (Zhou and Ling, 1998; Gillespie et al., 2006). Consistent with these studies, we did not observe any CGRP-IR intramural neurons in our study.

Conclusions

Our study has demonstrated that artemin potentially has three main targets in the bladder: the detrusor, suburothelial plexus and vasculature. GFRα3 immunohistochemistry labeled very specific populations of axons and non-neuronal cells, targeting distinct groups of peptidergic afferent axons, sympathetic noradrenergic vasoconstrictor axons and glia. We have also provided evidence that NF200-IR is found in bladder-projecting autonomic neurons, and identified distinctive structural features within axons of different chemical classes.

Supplementary Material

Refer to Web version on PubMed Central for supplementary material.

Acknowledgments

This study was supported by Award Number R01DK069351 from the National Institute of Diabetes and Digestive and Kidney Diseases (NIDDK). The content is solely the responsibility of the authors and does not necessarily represent the official views of the NIDDK or the National Institutes of Health. It was also supported by Project Grants 1003512 and 1022941, and Senior Research Fellowship 632903 from the National Health and Medical Research Council of Australia.

Literature cited

Airaksinen MS, Saarma M. The GDNF family: signalling, biological functions and therapeutic value. Nat Rev Neurosci. 2002; 3:383–394. [PubMed: 11988777]

Alian M, Gabella G. Decrease and disappearance of intramural neurons in the rat bladder during post-natal development. Neurosci Lett. 1996; 218:103–106. [PubMed: 8945738]

Alm P, Uvelius B, Ekstrom J, Holmqvist B, Larsson B, Andersson KE. Nitric oxide synthase-containing neurons in rat parasympathetic, sympathetic and sensory ganglia: a comparative study. Histochem J. 1995a; 27:819–831. [PubMed: 8575944]

Alm P, Zygmunt PK, Iselin C, Larsson B, Uvelius B, Werner S, Andersson KE. Nitric oxide synthase-immunoreactive, adrenergic, cholinergic, and peptidergic nerves of the female rat urinary tract: a comparative study. J Auton Nerv Syst. 1995b; 56:105–114. [PubMed: 8786272]

Andres R, Forgie A, Wyatt S, Chen Q, de Sauvage FJ, Davies AM. Multiple effects of artemin on sympathetic neurone generation, survival and growth. Development. 2001; 128:3685–3695. [PubMed: 11585795]

Baloh RH, Tansey MG, Lampe PA, Fahrner TJ, Enomoto H, Simburger KS, Leitner ML, Araki T, Johnson EM Jr, Milbrandt J. Artemin, a novel member of the GDNF ligand family, supports peripheral and central neurons and signals through the GFRalpha3-RET receptor complex. Neuron. 1998; 21:1291–1302. [PubMed: 9883723]

Bennett DL, Boucher TJ, Armanini MP, Poulsen KT, Michael GJ, Priestley JV, Phillips HS, McMahon SB, Shelton DL. The glial cell line-derived neurotrophic factor family receptor components are differentially regulated within sensory neurons after nerve injury. J Neurosci. 2000; 20:427–437. [PubMed: 10627618]

Bennett DL, Boucher TJ, Michael GJ, Popat RJ, Malcangio M, Averill SA, Poulsen KT, Priestley JV, Shelton DL, McMahon SB. Artemin has potent neurotrophic actions on injured C-fibres. J Peripher Nerv Syst. 2006; 11:330–345. [PubMed: 17117942]

Bennett DL, Michael GJ, Ramachandran N, Munson JB, Averill S, Yan Q, McMahon SB, Priestley JV. A distinct subgroup of small DRG cells express GDNF receptor components and GDNF is protective for these neurons after nerve injury. J Neurosci. 1998; 18:3059–3072. [PubMed: 9526023]

Bespalov MM, Saarma M. GDNF family receptor complexes are emerging drug targets. Trends Pharmacol Sci. 2007; 28:68–74. [PubMed: 17218019]

Callsen-Cencic P, Mense S. Expression of neuropeptides and nitric oxide synthase in neurons innervating the inflamed rat urinary bladder. J Auton Nerv Syst. 1997; 65:33–44. [PubMed: 9258870]

Chao T, Pham K, Steward O, Gupta R. Chronic nerve compression injury induces a phenotypic switch of neurons within the dorsal root ganglia. J Comp Neurol. 2008; 506:180–193. [PubMed: 18022951]

Cheng C, Guo GF, Martinez JA, Singh V, Zochodne DW. Dynamic plasticity of axons within a cutaneous milieu. J Neurosci. 2010; 30:14735–14744. [PubMed: 21048132]

Chiocchetti R, Bombardi C, Mongardi-Fantaguzzi C, Venturelli E, Russo D, Spadari A, Montoneri C, Romagnoli N, Grandis A. Intrinsic innervation of the horse ileum. Res Vet Sci. 2009; 87:177–185. [PubMed: 19380154]

Coelho A, Cruz F, Cruz CD, Avelino A. Effect of onabotulinumtoxinA on intramural parasympathetic ganglia: an experimental study in the guinea pig bladder. J Urol. 2012; 187:1121–1126. [PubMed: 22266001]

Damon DH, Teriele JA, Marko SB. Vascular-derived artemin: a determinant of vascular sympathetic innervation? Am J Physiol Heart Circ Physiol. 2007; 293:H266–273. [PubMed: 17337595]

Davidson RA, McCloskey KD. Morphology and localization of interstitial cells in the guinea pig bladder: structural relationships with smooth muscle and neurons. J Urol. 2005; 173:1385–1390. [PubMed: 15758810]

Ding YQ, Wang YQ, Qin BZ, Li JS. The major pelvic ganglion is the main source of nitric oxide synthase-containing nerve fibers in penile erectile tissue of the rat. Neurosci Lett. 1993; 164:187–189. [PubMed: 7512245]

Dixon JS, Gilpin SA, Gilpin CJ, Gosling JA. Intramural ganglia of the human urinary bladder. Br J Urol. 1983; 55:195–198. [PubMed: 6839094]

Dobolyi A, Irwin S, Makara G, Usdin TB, Palkovits M. Calcitonin gene-related peptide-containing pathways in the rat forebrain. J Comp Neurol. 2005; 489:92–119. [PubMed: 15977170]

el-Badawi A, Schenk EA. Dual innervation of the mammalian urinary bladder. A histochemical study of the distribution of cholinergic and adrenergic nerves. Am J Anat. 1966; 119:405–427. [PubMed: 5972731]

Elitt CM, McIlwrath SL, Lawson JJ, Malin SA, Molliver DC, Cornuet PK, Koerber HR, Davis BM, Albers KM. Artemin overexpression in skin enhances expression of TRPV1 and TRPA1 in cutaneous sensory neurons and leads to behavioral sensitivity to heat and cold. J Neurosci. 2006; 26:8578–8587. [PubMed: 16914684]

Enamoto H, Heuckeroth RO, Golden JP, Johnson EMJ, Milbrandt J. Development of cranial parasympathetic ganglia requires sequential actions of GDNF and neurturin. Development. 2000; 127:4877–4889. [PubMed: 11044402]

Ernsberger U. The role of GDNF family ligand signalling in the differentiation of sympathetic and dorsal root ganglion neurons. Cell Tissue Res. 2008; 333:353–371. [PubMed: 18629541]

Ernsberger U. Role of neurotrophin signalling in the differentiation of neurons from dorsal root ganglia and sympathetic ganglia. Cell Tissue Res. 2009; 336:349–384. [PubMed: 19387688]

Faggian L, Pampinella F, Roelofs M, Paulon T, Franch R, Chiavegato A, Sartore S. Phenotypic changes in the regenerating rabbit bladder muscle. Role of interstitial cells and innervation on smooth muscle cell differentiation. Histochem Cell Biol. 1998; 109:25–39. [PubMed: 9452953]

Feig SL, Haberly LB. Surface-associated astrocytes, not endfeet, form the glia limitans in posterior piriform cortex and have a spatially distributed, not a domain, organization. J Comp Neurol. 2011; 519:1952–1969. [PubMed: 21452238]

Forrest SL, Keast JR. Expression of receptors for glial cell line-derived neurotrophic factor family ligands in sacral spinal cord reveals separate targets of pelvic afferent fibres. J Comp Neurol. 2008; 506:989–1002. [PubMed: 18085594]

Forrest SL, Osborne PB, Keast JR. Characterization of bladder sensory neurons in the context of myelination, receptors for pain modulators, and acute responses to bladder inflammation. Frontiers in neuroscience. 2013; 7:206. [PubMed: 24223534]

Gabella G. Intramural neurons in the urinary bladder of the guinea-pig. Cell Tissue Res. 1990; 261:231–237. [PubMed: 2401001]

Gabella G, Davis C. Distribution of afferent axons in the bladder of rats. J Neurocytol. 1998; 27:141–155. [PubMed: 10640174]

Gardell LR, Wang R, Ehrenfels C, Ossipov MH, Rossomando AJ, Miller S, Buckley C, Cai AK, Tse A, Foley SF, Gong B, Walus L, Carmillo P, Worley D, Huang C, Engber T, Pepinsky B, Cate RL, Vanderah TW, Lai J, Sah DW, Porreca F. Multiple actions of systemic artemin in experimental neuropathy. Nat Med. 2003; 9:1383–1389. [PubMed: 14528299]

Gibbins IL. Vasoconstrictor, vasodilator and pilomotor pathways in sympathetic ganglia of guinea-pigs. Neuroscience. 1992; 47:657–672. [PubMed: 1374857]

Gillespie JI, Markerink-van Ittersum M, De Vente J. Interstitial cells and cholinergic signalling in the outer muscle layers of the guinea-pig bladder. BJU Int. 2006; 97:379–385. [PubMed: 16430651]

Glebova NO, Ginty DD. Growth and survival signals controlling sympathetic nervous system development. Annual review of neuroscience. 2005; 28:191–222.

Goldshmit Y, Galea MP, Bartlett PF, Turnley AM. EphA4 regulates central nervous system vascular formation. J Comp Neurol. 2006; 497:864–875. [PubMed: 16802330]

Grol S, van Koeveringe GA, de Vente J, van Kerrebroeck PE, Gillespie JI. Regional differences in sensory innervation and suburothelial interstitial cells in the bladder neck and urethra. BJU Int. 2008; 102:870–877. [PubMed: 18537955]

Hayashi T, Kondo T, Ishimatsu M, Yamada S, Nakamura K, Matsuoka K, Akasu T. Expression of the TRPM8-immunoreactivity in dorsal root ganglion neurons innervating the rat urinary bladder. Neurosci Res. 2009; 65:245–251. [PubMed: 19622375]

Heuckeroth RO, Enomoto H, Grider JR, Golden JP, Hanke JA, Jackman A, Molliver DC, Bardgett ME, Snider WD, Johnson EM Jr, Milbrandt J. Gene targeting reveals a critical role for neurturin in the development and maintenance of enteric, sensory, and parasympathetic neurons. Neuron. 1999; 22:253–263. [PubMed: 10069332]

Honma Y, Araki T, Gianino S, Bruce A, Heuckeroth R, Johnson E, Milbrandt J. Artemin is a vascular-derived neurotropic factor for developing sympathetic neurons. Neuron. 2002; 35:267–282. [PubMed: 12160745]

Iuchi H, Satoh Y, Ono K. Postnatal development of neuropeptide Y- and calcitonin gene-related peptide-immunoreactive nerves in the rat urinary bladder. Anat Embryol (Berl). 1994; 189:361–373. [PubMed: 8074324]

Ivanusic JJ. Size, neurochemistry, and segmental distribution of sensory neurons innervating the rat tibia. J Comp Neurol. 2009; 517:276–283. [PubMed: 19757492]

Kalous A, Osborne PB, Keast JR. Spinal cord compression injury in adult rats initiates changes in dorsal horn remodeling that may correlate with development of neuropathic pain. J Comp Neurol. 2009; 513:668–684. [PubMed: 19235905]

Keast JR. Plasticity of pelvic autonomic ganglia and urogenital innervation. Int Rev Cytol. 2006; 248:141–208. [PubMed: 16487791]

Keast JR, de Groat WC. Immunohistochemical characterization of pelvic neurons which project to the bladder, colon, or penis in rats. J Comp Neurol. 1989; 288:387–400. [PubMed: 2571623]

Keast JR, Forrest SL, Osborne PB. Sciatic nerve injury in adult rats causes distinct changes in the central projections of sensory neurons expressing different glial cell line-derived neurotrophic factor family receptors. J Comp Neurol. 2010; 518:3024–3045. [PubMed: 20533358]

Lawson SN, Perry MJ, Prabhakar E, McCarthy PW. Primary sensory neurones: neurofilament, neuropeptides, and conduction velocity. Brain Res Bull. 1993; 30:239–243. [PubMed: 7681350]

Lee SJ, Kirigiti M, Lindsley SR, Loche A, Madden CJ, Morrison SF, Smith MS, Grove KL. Efferent projections of neuropeptide Y-expressing neurons of the dorsomedial hypothalamus in chronic hyperphagic models. J Comp Neurol. 2013; 521:1891–1914. [PubMed: 23172177]

Llewellyn-Smith IJ, Gnanamanickam GJ. Immunoperoxidase detection of neuronal antigens in full-thickness whole mount preparations of hollow organs and thick sections of central nervous tissue. J Neurosci Methods. 2010; 196:1–11. [PubMed: 21167203]

Malin SA, Molliver DC, Koerber HR, Cornuet P, Frye R, Albers KM, Davis BM. Glial cell line-derived neurotrophic factor family members sensitize nociceptors in vitro and produce thermal hyperalgesia in vivo. J Neurosci. 2006; 26:8588–8599. [PubMed: 16914685]

Mattiasson A, Ekblad E, Sundler F, Uvelius B. Origin and distribution of neuropeptide Y-, vasoactive intestinal polypeptide-and substance P-containing nerve fibers in the urinary bladder of the rat. Cell Tissue Res. 1985; 239:141–146. [PubMed: 2578316]

McCloskey KD. Interstitial cells in the urinary bladder--localization and function. Neurourol Urodyn. 2010; 29:82–87. [PubMed: 20025023]

McIlvried LA, Albers K, Gold MS. Distribution of artemin and GFRalpha3 labeled nerve fibers in the dura mater of rat: artemin and GFRalpha3 in the dura. Headache. 2010; 50:442–450. [PubMed: 19845789]

Molliver DC, Radeke MJ, Feinstein SC, Snider WD. Presence or absence of TrkA protein distinguishes subsets of small sensory neurons with unique cytochemical characteristics and dorsal horn projections. J Comp Neurol. 1995; 361:404–416. [PubMed: 8550888]

Orozco OE, Walus L, Sah DW, Pepinsky RB, Sanicola M. GFRalpha3 is expressed predominantly in nociceptive sensory neurons. Eur J Neurosci. 2001; 13:2177–2182. [PubMed: 11422460]

Robertson B, Perry MJ, Lawson SN. Populations of rat spinal primary afferent neurons with choleragenoid binding compared with those labelled by markers for neurofilament and carbohydrate groups: a quantitative immunocytochemical study. J Neurocytol. 1991; 20:387–395. [PubMed: 1869879]

Ruan HZ, Birder LA, Xiang Z, Chopra B, Buffington T, Tai C, Roppolo JR, de Groat WC, Burnstock G. Expression of P2X and P2Y receptors in the intramural parasympathetic ganglia of the cat urinary bladder. Am J Physiol Renal Physiol. 2006; 290:F1143–1152. [PubMed: 16332929]

Russo D, Clavenzani P, Sorteni C, Bo Minelli L, Botti M, Gazza F, Panu R, Ragionieri L, Chiocchetti R. Neurochemical features of boar lumbo-sacral dorsal root ganglion neurons and characterization of sensory neurons innervating the urinary bladder trigone. J Comp Neurol. 2013; 521:342–366. [PubMed: 22740069]

Scherrer G, Low SA, Wang X, Zhang J, Yamanaka H, Urban R, Solorzano C, Harper B, Hnasko TS, Edwards RH, Basbaum AI. VGLUT2 expression in primary afferent neurons is essential for normal acute pain and injury-induced heat hypersensitivity. Proc Natl Acad Sci U S A. 2010

Skalli O, Ropraz P, Trzeciak A, Benzonana G, Gillessen D, Gabbiani G. A monoclonal antibody against alpha-smooth muscle actin: a new probe for smooth muscle differentiation. J Cell Biol. 1986; 103:2787–2796. [PubMed: 3539945]

Smet PJ, Edyvane KA, Jonavicius J, Marshall VR. Neuropeptides and neurotransmitter-synthesizing enzymes in intrinsic neurons of the human urinary bladder. J Neurocytol. 1996; 25:112–124. [PubMed: 8699193]

Springer JE, Mu X, Bergmann LW, Trojanowski JQ. Expression of GDNF mRNA in rat and human nervous tissue. Exp Neurol. 1994; 127:167–170. [PubMed: 8033959]

Tanaka T, Shinoda M, Feng B, Albers KM, Gebhart GF. Modulation of visceral hypersensitivity by glial cell line-derived neurotrophic factor family receptor α-3 in colorectal afferents. American journal of physiology Gastrointestinal and liver physiology. 2011; 300:G418–424. [PubMed: 21193524]

Trojanowski JQ, Walkenstein N, Lee VM. Expression of neurofilament subunits in neurons of the central and peripheral nervous system: an immunohistochemical study with monoclonal antibodies. J Neurosci. 1986; 6:650–660. [PubMed: 2420946]

Trupp M, Belluardo N, Funakoshi H, Ibanez CF. Complementary and overlapping expression of glial cell line-derived neurotrophic factor (GDNF), c-ret proto-oncogene, and GDNF receptor-alpha indicates multiple mechanisms of trophic actions in the adult rat CNS. J Neurosci. 1997; 17:3554–3567. [PubMed: 9133379]

Vessey KA, Wilkinson-Berka JL, Fletcher EL. Characterization of retinal function and glial cell response in a mouse model of oxygen-induced retinopathy. J Comp Neurol. 2011; 519:506–527. [PubMed: 21192081]

Vizzard MA. Changes in urinary bladder neurotrophic factor mRNA and NGF protein following urinary bladder dysfunction. Exp Neurol. 2000; 161:273–284. [PubMed: 10683293]

Vizzard MA, Erdman SL, de Groat WC. Increased expression of neuronal nitric oxide synthase in bladder afferent pathways following chronic bladder irritation. J Comp Neurol. 1996; 370:191–202. [PubMed: 8808730]

Wakabayashi Y, Makiura Y, Tomoyoshi T, Kitahama K, Geffard M, Maeda T. Adrenergic innervation of the urinary bladder body in the cat with special reference to structure of the detrusor muscle: an immunohistochemical study of noradrenaline and its synthesizing enzymes. Arch Histol Cytol. 1994; 57:277–289. [PubMed: 7818951]

Wakabayashi Y, Makiura Y, Tomoyoshi T, Kitahama K, Maeda T. Immuno-electron microscopic study of tyrosine hydroxylase in the cat urinary bladder and proximal urethra. J Auton Nerv Syst. 1993; 44:243–252. [PubMed: 7901263]

Wang R, King T, Ossipov MH, Rossomando AJ, Vanderah TW, Harvey P, Cariani P, Frank E, Sah DW, Porreca F. Persistent restoration of sensory function by immediate or delayed systemic artemin after dorsal root injury. Nat Neurosci. 2008; 11:488–496. [PubMed: 18344995]

Wang R, Rossomando A, Sah DW, Ossipov MH, King T, Porreca F. Artemin induced functional recovery and reinnervation after partial nerve injury. Pain. 2014; 155:476–484. [PubMed: 24269493]

Wang T, Molliver DC, Jing X, Schwartz ES, Yang FC, Samad OA, Ma Q, Davis BM. Phenotypic switching of nonpeptidergic cutaneous sensory neurons following peripheral nerve injury. PLoS One. 2011; 6:e28908. [PubMed: 22216140]

Warburton AL, Santer RM. Sympathetic and sensory innervation of the urinary tract in young adult and aged rats: a semi-quantitative histochemical and immunohistochemical study. Histochem J. 1994; 26:127–133. [PubMed: 7908663]

Yang C, Hutto D, Sah DW. Distribution of GDNF family receptor alpha3 and RET in rat and human non-neural tissues. J Mol Histol. 2006; 37:69–77. [PubMed: 16773224]

Yokokawa K, Tohyama M, Shiosaka S, Shiotani Y, Sonoda T, Emson PC, Hillyard CV, Girgis S, MacIntyre I. Distribution of calcitonin gene-related peptide-containing fibers in the urinary bladder of the rat and their origin. Cell Tissue Res. 1986; 244:271–278. [PubMed: 2424603]

Zagorodnyuk VP, Brookes SJ, Spencer NJ. Structure-function relationship of sensory endings in the gut and bladder. Auton Neurosci. 2010; 153:3–11. [PubMed: 19682956]

Zagorodnyuk VP, Brookes SJ, Spencer NJ, Gregory S. Mechanotransduction and chemosensitivity of two major classes of bladder afferents with endings in the vicinity to the urothelium. The Journal of physiology. 2009; 587:3523–3538. [PubMed: 19470774]

Zhang L, Ma Z, Smith GM, Wen X, Pressman Y, Wood PM, Xu XM. GDNF-enhanced axonal regeneration and myelination following spinal cord injury is mediated by primary effects on neurons. Glia. 2009; 57:1178–1191. [PubMed: 19170182]

Zhou Y, Ling EA. Colocalization of nitric oxide synthase and some neurotransmitters in the intramural ganglia of the guinea pig urinary bladder. J Comp Neurol. 1998; 394:496–505. [PubMed: 9590557]

Zvarova K, Vizzard MA. Distribution and fate of cocaine- and amphetamine-regulated transcript peptide (CARTp)-expressing cells in rat urinary bladder: a developmental study. J Comp Neurol. 2005; 489:501–517. [PubMed: 16025456]

Zylka MJ, Rice FL, Anderson DJ. Topographically distinct epidermal nociceptive circuits revealed by axonal tracers targeted to Mrgprd. Neuron. 2005; 45:17–25. [PubMed: 15629699]

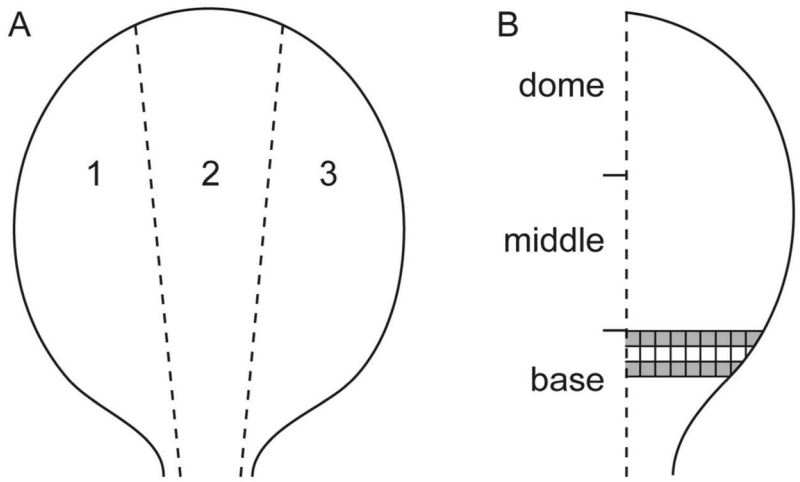

Figure 1.

Diagram of bladder whole mount preparation. **A.** The bladder was cut into three longitudinal strips of approximately equal size. **B.** Areas of interest (AOI; shaded boxes) were assessed for GFRα3- and CGRP-immunoreactive (IR) terminals in the suburothelial plexus and for CGRP- and TH-IR terminals in the detrusor. Dimensions of each box were 500 × 500 μm. CGRP, calcitonin gene-related peptide; GFRα3, glial cell line-derived neurotrophic factor family receptor α3; TH, tyrosine hydroxylase.

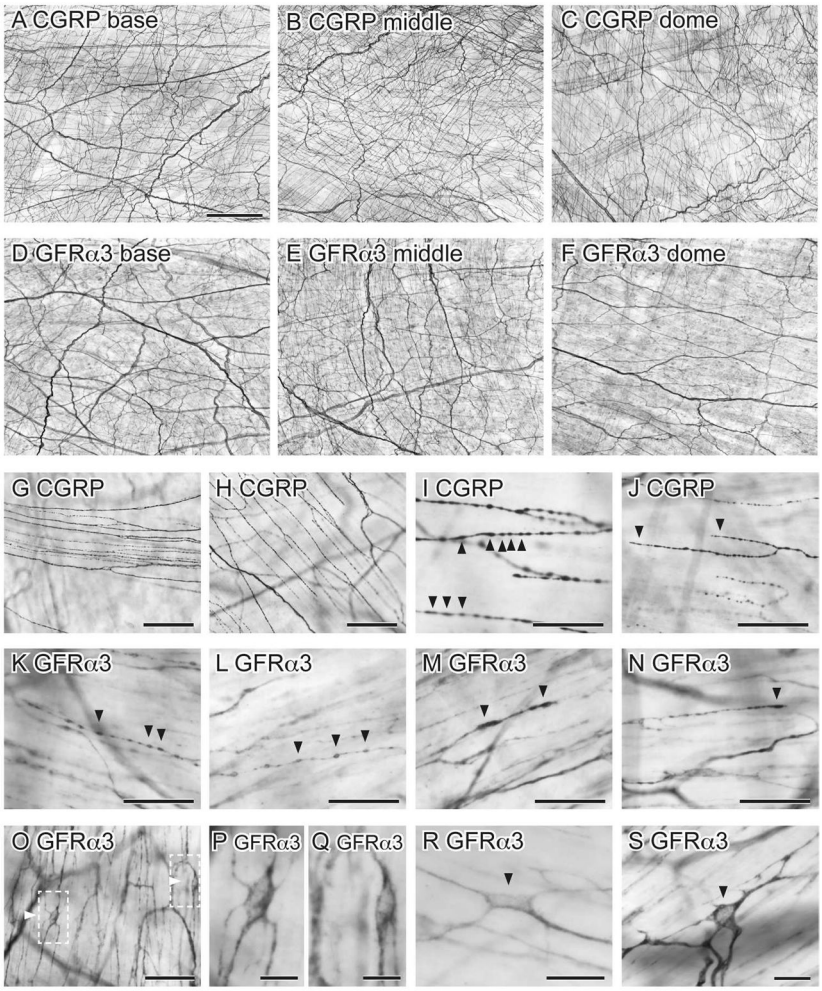

Figure 2.

Distribution of CGRP- and GFRα3-immunoreactivity (IR) in the detrusor of whole mounts processed with diaminobenzidine. **A–F** show low magnification images to illustrate the density of axons in different regions of the bladder. There was no obvious difference in axon density between base, middle and dome of bladder for CGRP-IR (**A–C**) or GFRα3-IR (**D–F**) axons. Higher magnification images of axons are shown in **G–N. G, H**: Thin bundles and single CGRP-IR axons running parallel to muscle bundles; **I, J**: Single CGRP-IR axons showed numerous varicosities and unspecialised points of termination. **K–N**: Single GFRα3-IR axons had a similar varicose structure to those labelled for CGRP. **O–S**: Numerous small GFRα3-IR cells were observed in the detrusor. Arrowheads show varicosities (I, K–M) and terminals (J, N) and GFRα3-IR cells (O, R, S). Dashed boxes in (O) are magnified in (P) and (Q). Scale bar in (A) represents 500 μm also applies to (B–F). Other scale bars represent 100 μm (G, H, J), 50 μm (I, K–O), 20 μm (R) or 10 μm (P, Q, S). CGRP, calcitonin gene-related peptide; GFRα3, glial cell line-derived neurotrophic factor family receptor α3.

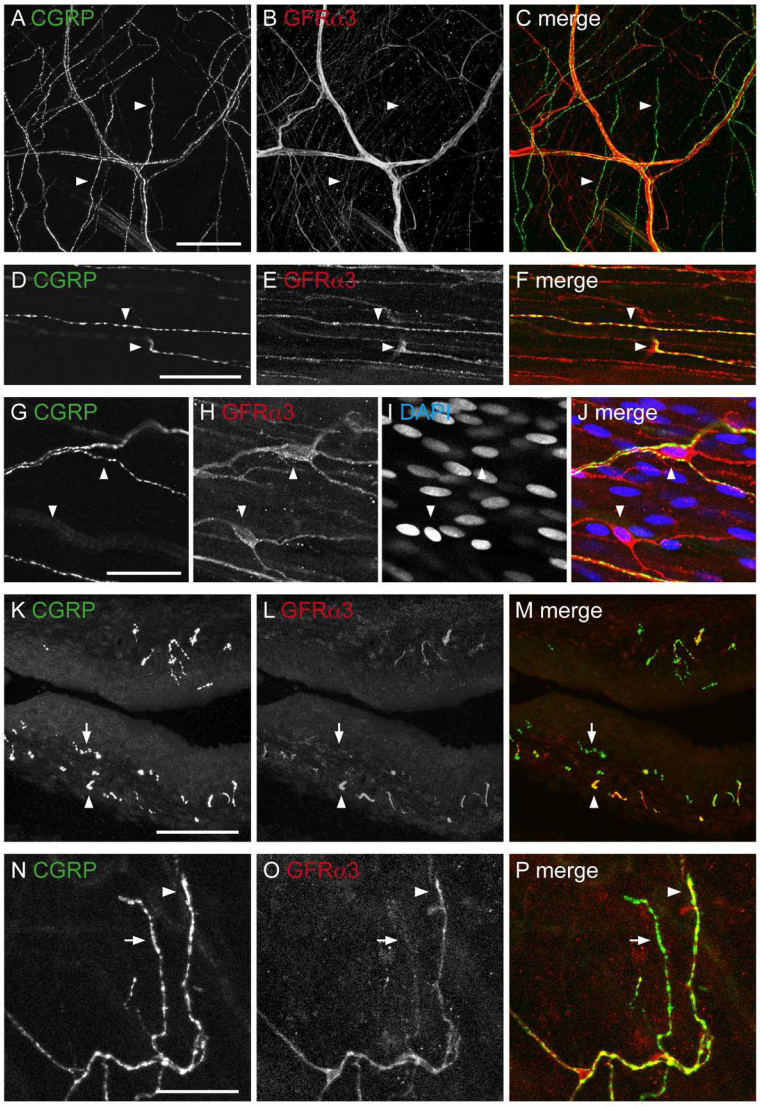

Figure 3.

Co-expression of CGRP- and GFRα3-immunoreactivity (IR) in the detrusor and suburothelial plexus. All panels except K–M (cryosection) are from whole mount preparations. **A–C:** Confocal z-stack (34 μm thick, 1 μm step size) through the detrusor showed that many CGRP-IR axon bundles contained GFRα3-IR axons, but some single axons labeled for CGRP-IR were GFRα3-negative (arrowheads). **D–F:** Confocal image in the detrusor illustrating partial co-expression (arrowheads) between CGRP- and GFRα3-IR in axons. **G–J:** Confocal image in the detrusor showing two small, elongated GFRα3-IR cells (arrowheads) with their processes. These appeared to be innervated by CGRP axons. DAPI (blue) labels nuclei of GFRα3-IR cells and surrounding muscle cells. **K–M:** Confocal z-stack (15 μm thick, 0.5 μm step size) of a cryosection showing the majority of GFRα3-IR axons in the suburothelial plexus were immunoreactive for CGRP but relatively few CGRP-IR axons were immunoreactive for GFRα3. **N–P:** Confocal images in the suburothelial plexus of a whole mount demonstrating that most GFRα3-IR terminals were

immunoreactive for CGRP, but some CGRP-IR terminals were not immunoreactive for GFRα3. In K–P, arrows indicate single-labeled CGRP-IR axons (K–M) and terminals (N–P), whereas arrowheads indicate a double-labeled GFRα3- and CGRP-IR axon (k–m), and terminal (n–p). Scale bar = 100 μm in (A) also applies to (B, C); 30 μm in (D) also applies to (E, F); 20 μm in (G) also applies to (H–J). Scale bar = 100 μm in (K) also applies to (L–M); 30 μm in (N) also applies to (O, P). CGRP, calcitonin gene-related peptide; GFRα3, glial cell line-derived neurotrophic factor family receptor α3.

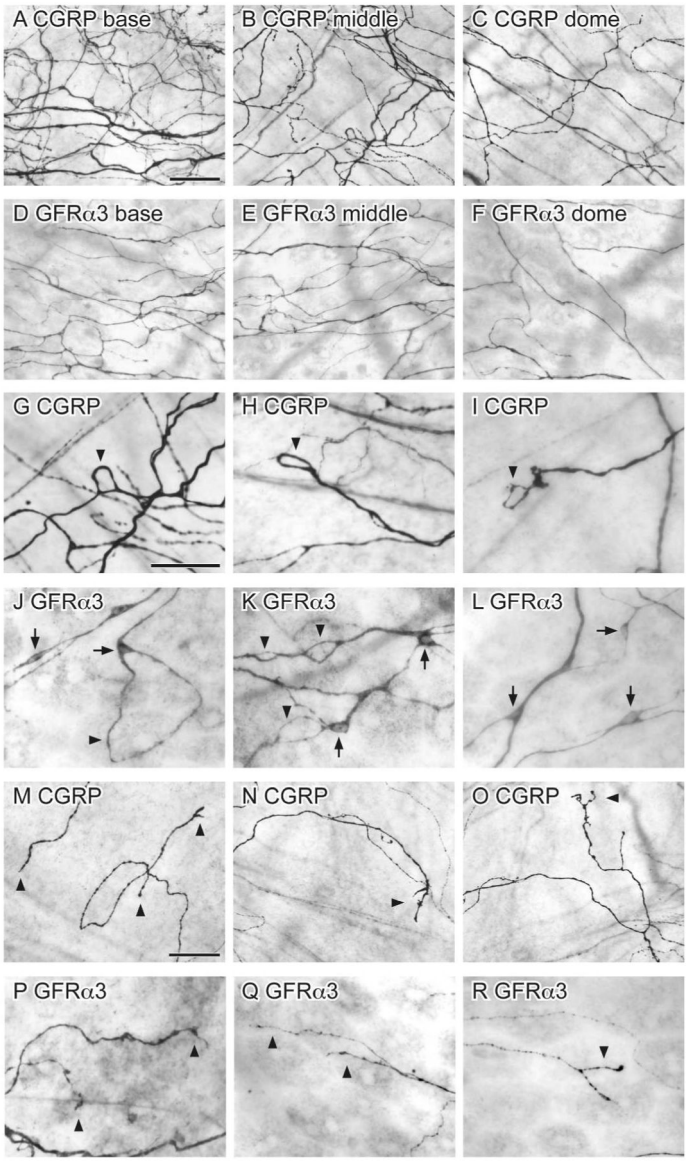

Figure 4.

Distribution of CGRP- and GFRα3-immunoreactivity (IR) in the suburothelial plexus of whole mounts processed with diaminobenzidine (DAB). **A–F:** CGRP- (A–C) and GFRα3-IR (D–F) axons in the suburothelial plexus became progressively less dense towards the bladder dome (A, D: base; B, E: middle; C, F: dome). **G–I:** CGRP-IR axons formed closed loops (arrowheads) originating in the middle of axons (G) or on axon terminals (H, I). **J, K:** GFRα3-IR axons also formed closed loops (arrowheads) at the end of terminating axons (J) or in the middle of axons (K). **J–L:** Numerous small GFRα3-IR cells (arrows) were observed close to axons in the suburothelial plexus. **M–R:** CGRP-IR (M–O) and GFRα3-IR (P–R) terminals (arrowheads) in the suburothelial plexus. Scale bar = 100 μm in (A) also applies to (B–F); 50 μm in (G) also applies to (H–L); 50 μm in (M) also applies to (N–R). CGRP, calcitonin gene-related peptide; GFRα3, glial cell line-derived neurotrophic factor family receptor α3.

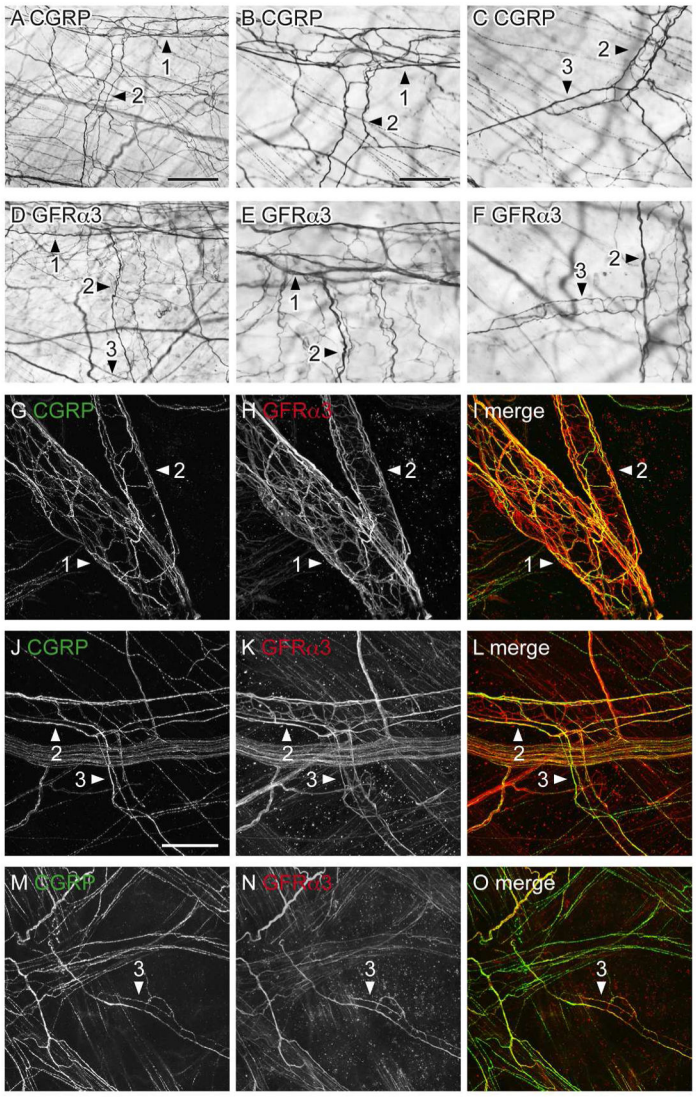

Figure 5.

CGRP- and GFRα3-immunoreactive (IR) axons associated with the bladder vasculature as viewed in whole mounts. Panels **A–F** show diaminobenzidine (DAB)-processed tissue viewed with conventional microscopy whereas **G–O** are confocal micrographs of immunofluorescence. Numbered arrowheads indicate primary, secondary and tertiary branches of the vascular tree. **A–C:** Many CGRP-IR para-vascular axons were found on the primary, secondary (A, B) and tertiary (C) branches of the vascular tree; peri-vascular axons were also found on the primary branch but were sparse on subsequent branches. **D–F:** Para- and peri-vascular GFRα3-IR axons were associated with all branches of the vascular tree. **G–I:** Many para-vascular CGRP- and GFRα3-IR axons were associated with the primary and secondary branches of the vascular tree; GFRα3-IR peri-vascular axons were more prevalent than CGRP-IR peri-vascular axons on these branches. **J–I:** CGRP- and GFRα3-IR para-vascular axons were associated with secondary and tertiary vessel branches; many GFRα3-IR peri-vascular axons were present in these branches. **m–o:** Neither CGRP- nor GFRα3-IR para-vascular axons extended to the most distal aspects of the vascular tree.

Images (G–O) are confocal z-stacks (thickness: G–I, 45 μm; J–L, 28 μm; M–O, 30 μm; all with 1 μm step size). Scale bar = 200 μm in (A) also applies to (D); 100 μm in (B) also applies to (C, E, F); 100 μm in (g) also applies to (H, I); 100 μm (J) also applies (K, L); 100 μm in (M) also applies to (N, O). CGRP, calcitonin gene-related peptide; GFRα3, glial cell line-derived neurotrophic factor family receptor α3.

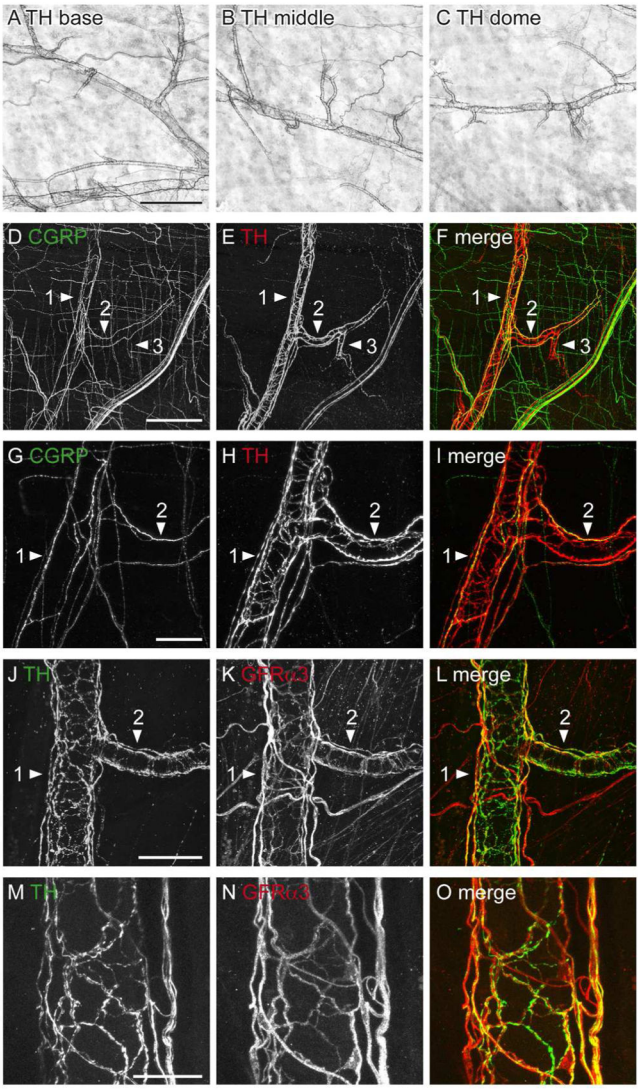

Figure 6.

Comparison of different axon populations supplying blood vessels in bladder whole mounts. Panels **A–C** show diaminobenzidine (DAB)-processed tissue viewed with conventional microscopy whereas **D–O** are confocal micrographs of immunofluorescence. Numbered arrowheads indicate primary, secondary and tertiary branches of the vascular tree. **A–C:** TH-immunoreactive (IR) axons densely innervated all branches of the vascular tree that traversed the bladder (A: base; B: middle; C: dome). **D–F:** Many TH-IR axons and relatively few CGRP-IR axons were associated with distal portions of primary vessel branches. **G–I:** Higher magnification of the primary to secondary branch point in d-f that demonstrates relatively few CGRP-IR peri-vascular axons. **J–L:** Numerous TH- and GFRα3-IR para- and peri-vascular axons densely innervated the primary and secondary branches of the vascular tree. **M–O:** Many TH-IR para- and peri-vascular axons were immunoreactive for GFRα3. Panels (D–O) are confocal z-stacks (thickness: D–F, 50 μm; g-l, 30–32 μm; all with 1 μm step size). Scale bar = 500 μm in (A) also applies to (B, C); 200 μm in (D) also applies to (E, F); 50 μm in (G) also applies to (H–L); 40 μm in (M) also

applies to (N–O). CGRP, calcitonin gene-related peptide; GFRα3, glial cell line-derived neurotrophic factor family receptor α3; TH, tyrosine hydroxylase.

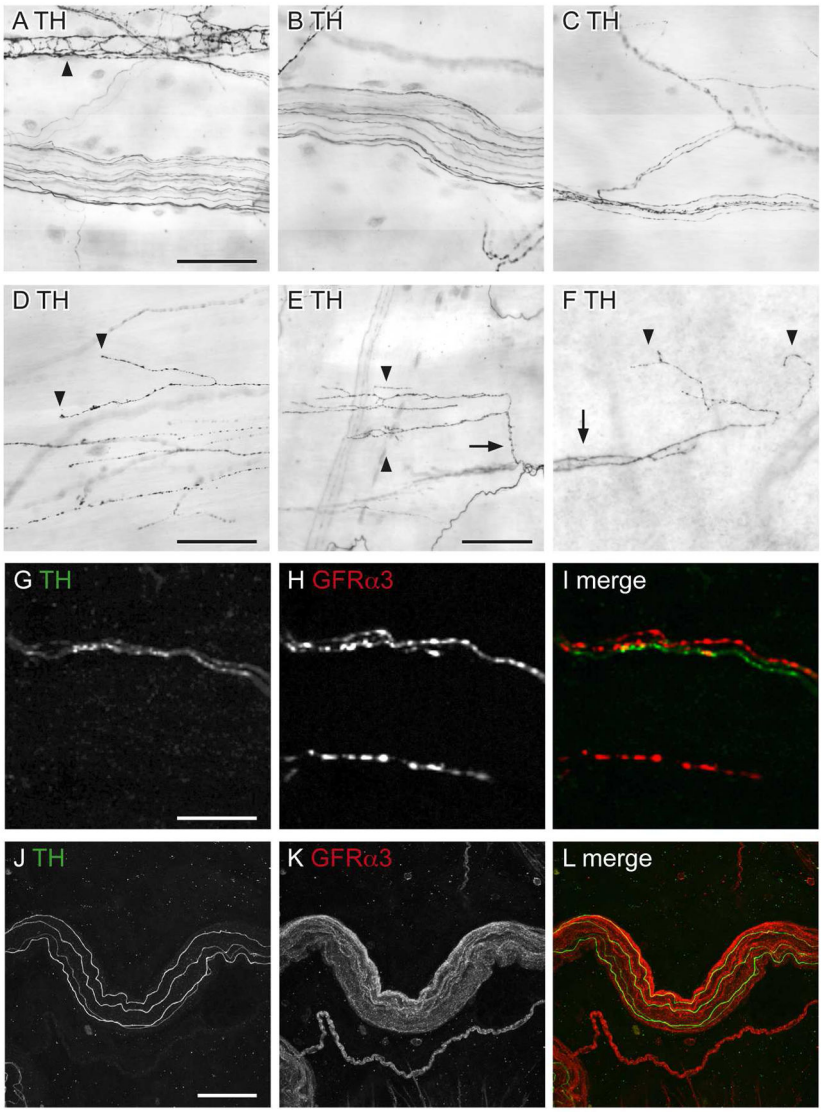

Figure 7.

Non-vascular noradrenergic innervation of the detrusor, as viewed in whole mount preparations. Panels **A–F** show diaminobenzidine (DAB)-processed tissue viewed with conventional microscopy whereas **G–L** are confocal micrographs of immunofluorescence. **A–C:** TH-immunoreactive (IR) axon bundles of varying thickness and axons associated with a blood vessel (arrowhead, A). **D–F:** Three types of TH-IR axon terminals (arrowheads) were found in the detrusor: non-specialised simple endings (D), specialised multi-branched endings (E), and those that branched off the vascular tree, originating from para-vascular axons (F). Arrows indicate a branch point from a single specialised TH-IR axon (E) and TH-IR para-vascular axons on a distal portion of the vascular tree (F). **G–I:** TH- and GFRα3-IR were rarely co-expressed in axons in the detrusor. **J–L:** Few TH-IR axons travelled within the large diameter bundles of GFRα3-IR axons; these TH-IR axons did not co-express GFRα3-IR. Images (G–O) are confocal z-stacks (thickness: G–I, 10 μm; J–L, 20 μm; all with 1 μm step size). Scale bar = 100 μm in (A) also applies to (B, C); 100 μm in (D) also

applies to (E, F); 10 μm in (G) also applies to (G, I); 50 μm in (J) also applies to (J, K, L). GFRα3, glial cell line-derived neurotrophic factor family receptor α3; TH, tyrosine hydroxylase.

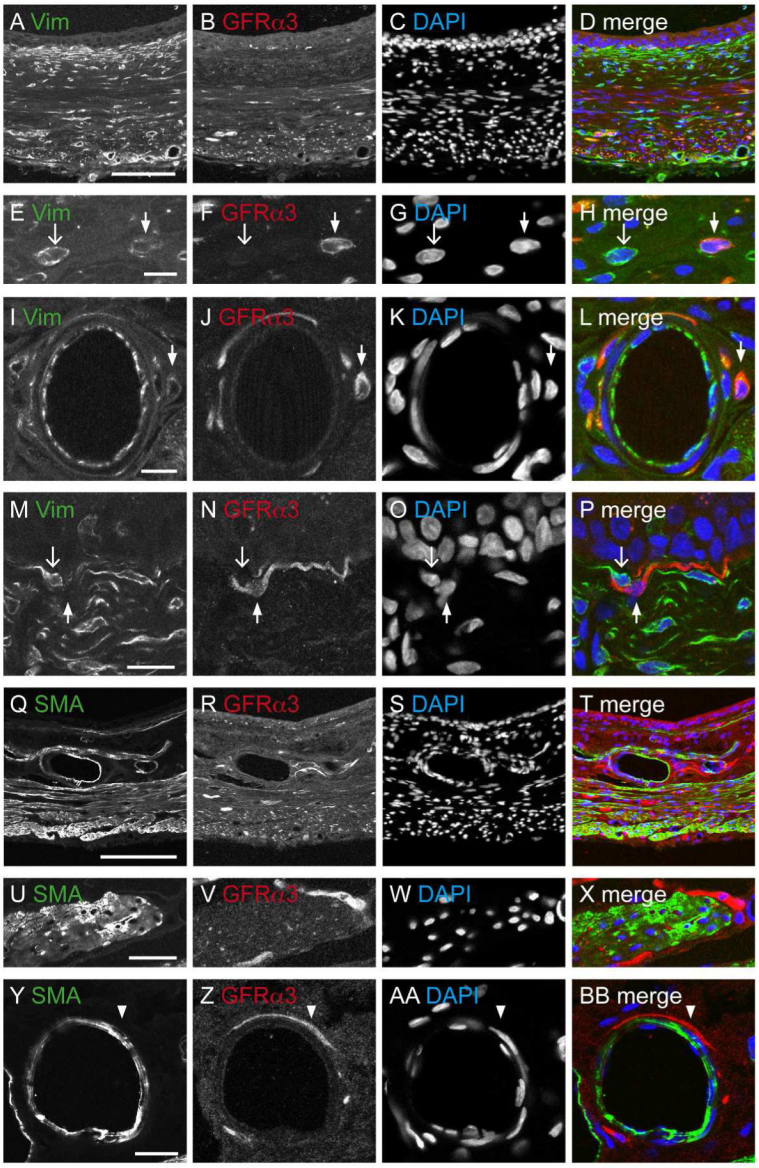

Figure 8.

Comparative distribution of vimentin- (Vim) and smooth muscle actin (SMA) with GFRα3-immunoreactivity (IR) in the bladder. All panels are confocal micrographs of immunofluorescence in bladder cryosections. DAPI labelling of nuclei was performed to indicate general cellular distribution within each tissue and to show that none of the other markers were found within the nucleus. The urothelial surface is orientated to the top in panels A–D, and M–T. **A–D:** Bladder base immunostained for Vim, GFRα3, and the merged image. **E–H:** Little co-expression occurred between Vim-IR and GFRα3-IR in cells in the detrusor. **I–L:**. GFRα3-IR cells associated with the vasculature were not immunoreactive for Vim. **M–P:** GFRα3- and Vim-IR were not co-expressed in the suburothelial tissue. In e-p, closed arrows indicate single-labeled GFRα3-IR cells and open arrows indicate single-labeled Vim-IR cells. **Q–T:** Bladder base comparing the distribution of SMA-, GFRα3-IR and the merged image. **U–X:** No co-expression of SMA- with GFRα3-

IR was observed in the detrusor. **Y-BB:** There was no coexpression of the SMA- and GFRα3-IR associated with the vasculature; arrowheads indicate single-labeled GFRα3-IR axons. Scale bar = 200 μm in (a) also applies to (B–D, Q–T); 10 μm in (E, I) also applies to (F–H, J–L); 30 μm in (U) also applies to (V–Y); 20 μm in (Y) also applies to (BB). GFRα3, glial cell line-derived neurotrophic factor family receptor α3.

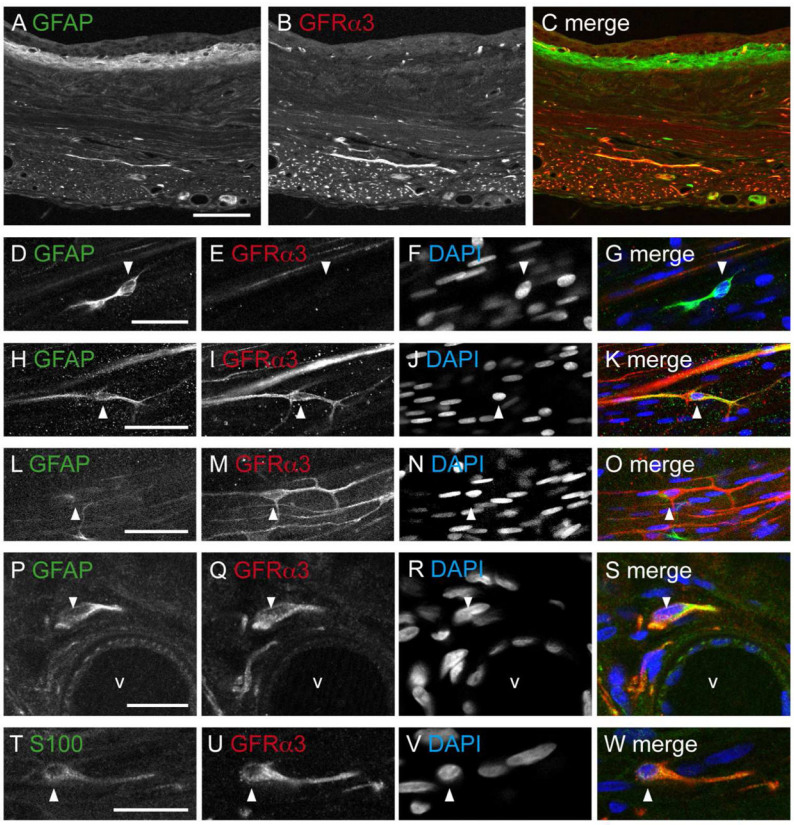

Figure 9.

Comparison of glial markers (GFAP- and S100-) with GFRα3-immunoreactive (IR) distribution in the bladder. Panels show confocal images of immunofluorescence in bladder sections (A–C, P–S) and wholemount preparations (D–O, T–W). DAPI labelling of nuclei was performed to indicate general cellular distribution within each tissue and to show that none of the other markers were found within the nucleus. **A–C:** Comparison of GFAP- and GFRα3-IR distribution in the bladder at low magnification. **D–G:** Many, but not all GFAP-IR cells in the detrusor were immunoreactive for GFRα3. **H–K:** Example of a double labelled GFAP- and GFRα3-IR glial cell in the detrusor. **L–O:** The majority of GFRα3-IR cells with elongated processes were not immunoreactive for GFAP. **P–S:** Many GFRα3-IR cells associated with the vasculature were immunoreactive for GFAP. **T–W:** Many S100-IR cells in the detrusor were immunoreactive for GFRα3. Arrowheads indicate single-labeled GFAP-IR cell (D–G), single-labeled GFRα3-IR cell (L–O), and double-labeled cells (H–K, P–S, T–W). The lumen of the blood vessel in panels P–S is indicated (V). Scale bar = 200 μm in (A) also applies (B, C); 20 μm in (D, H, L, T) also applies to (E–G, I–K, M–O, U–W); 10 μm in (P) also applies to (QS). GFAP, glial fibrillary acidic protein; GFRα3, glial cell line-derived neurotrophic factor family receptor α3.

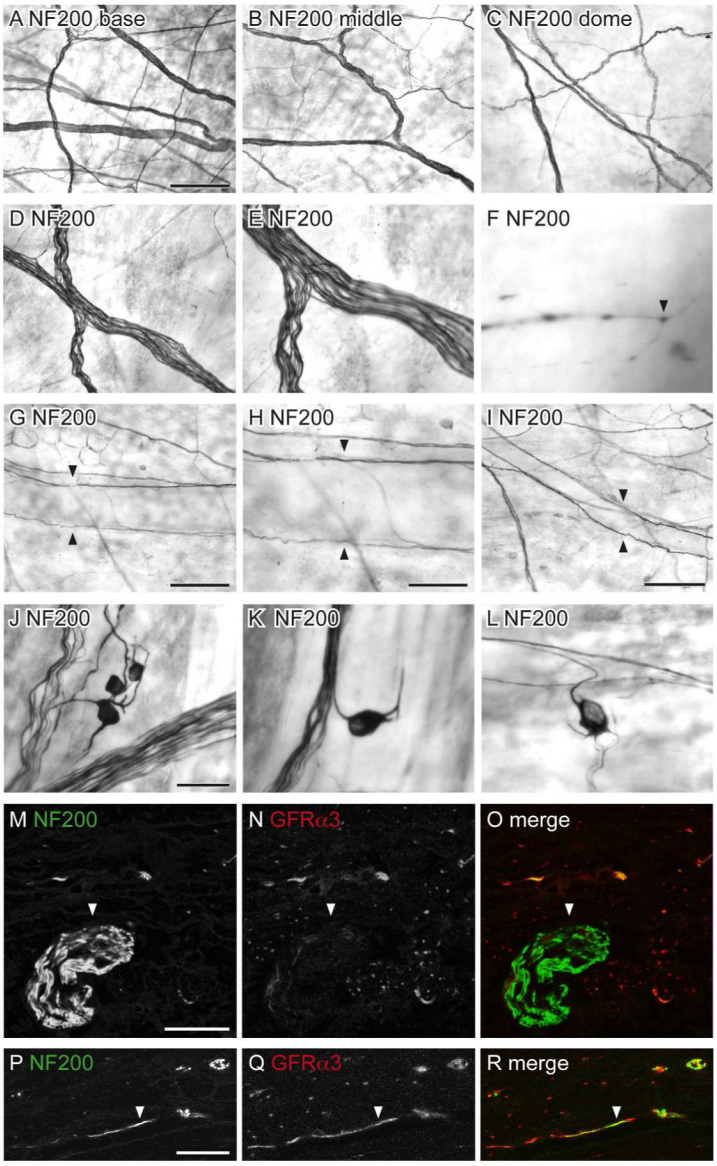

Figure 10.

Distribution of NF200-immunoreactive (IR) axons in the bladder. Panels **A–L** show DAB-processed whole mounts viewed with conventional microscopy whereas **M–R** are confocal micrographs of immunofluorescence in cryosections. **A–C:** Many NF200-IR axons were found in the detrusor and were distributed evenly throughout the bladder (a: base; b: middle; c: dome). **D–E:** The majority of NF200-IR axons travelled in large diameter axon bundles. **F:** NF200-IR terminals were occasionally observed in the detrusor (arrowhead). **G–I:** Few NF200-IR axons were associated with the vasculature; these were para-vascular (arrowheads) and only observed on primary (G, H) and secondary (I) vascular branches. **J–L:** NF200-IR neurons were observed in the detrusor; many had short processes and were found individually (K, L) or in small clusters (J). **M–O:** Large diameter NF200-IR axon bundles (arrowheads) on the serosal surface were not immunoreactive for GFRα3. **P–R:** Some NF200-IR axons in the detrusor were immunoreactive for GFRα3 (arrowheads); it

was difficult to determine if these comprised single or multiple axons. The serosal surface of the bladder is orientated to the bottom in panels m–r. Scale bar = 200 μm in (A) also applies to (B, C); 100 μm in (D) also applies to (E); 20 μm in (F); 200 μm in (G); 100 μm in (G); 200 μm in (I), 50 μm in (J) also applies to (K, L); 20 μm in (M) also applies to (N, O); 10 μm in (P) also applies (Q, R). GFRα3, glial cell line-derived neurotrophic factor family receptor α3; NF200, neurofilament, 200 kDa.

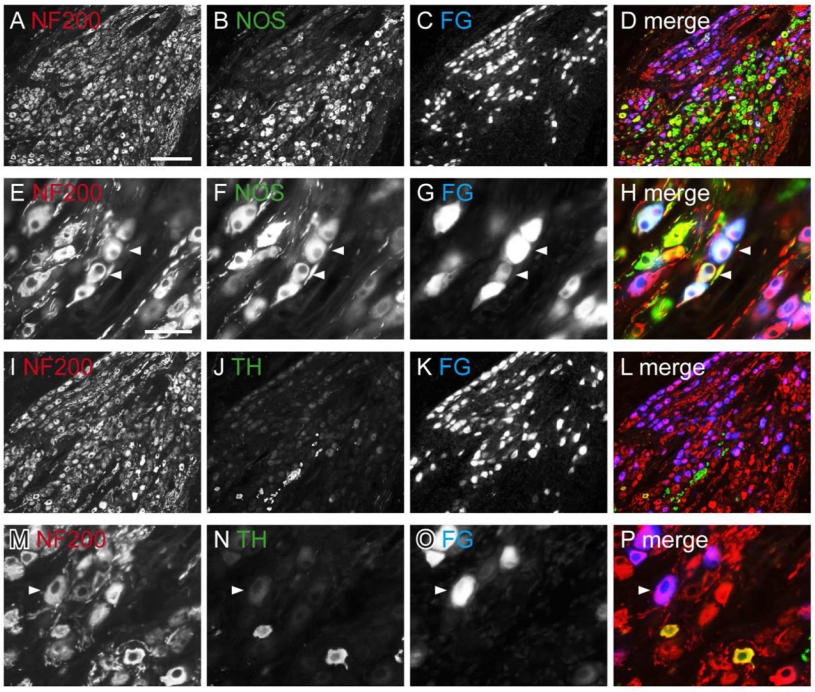

Figure 11.

Distribution of NF200-immunoreactivity (IR) in cryosections of pelvic ganglia, viewed with conventional fluorescence microscopy. Neurons containing retrograde tracer (FluoroGold; FG) have been colorised blue. FG neurons showing immunoreactivity for NF200-IR appear purple, and neurons containing FG with both immunolabels appear white. FG-negative neurons labelled for both substances appear yellow. **A–D:** Distribution of NF200-, NOS-IR and FG neurons in the pelvic ganglion. **E–H:** Co-expression of NF200- and NOS-IR in FG-labeled neurons (examples of coexpression shown with arrowheads). **I–L:** Distribution of NF200-, TH-IR and FG-labeled neurons in the pelvic ganglion, showing scarcity of TH-IR neurons. **M–P:** Expression of NF200- in TH-negative, FG-labeled neurons; arrowhead shows an NF200-IR FG neuron that does not show TH-IR; note that there are two neurons that express both TH- and NF200-IR but are FG-negative. Scale bar = 200 μm in (A) also applies to (B–D, I–L); 50 μm in (E) also applies to (F–H, M–P). NF200, neurofilament, 200 kDa; NOS, nitric oxide synthase; TH, tyrosine hydroxylase.

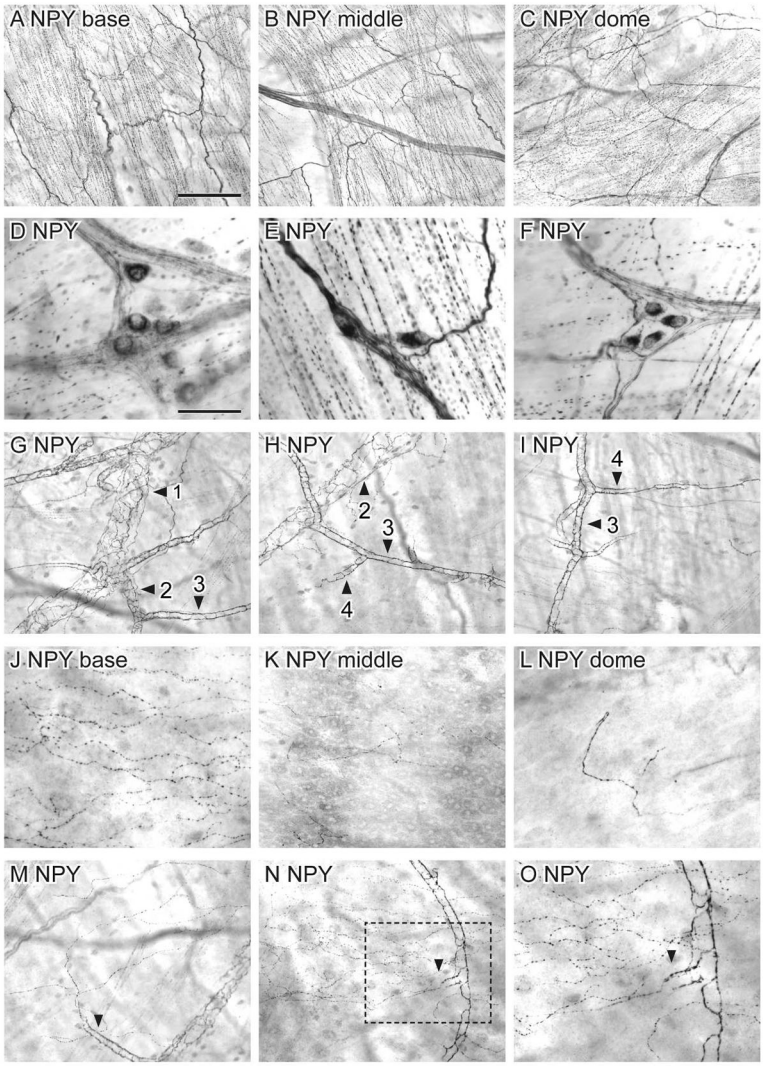

Figure 12.

Distribution of neuropeptide Y (NPY)-immunoreactivity (IR) in the bladder, viewed using diaminobenzidine (DAB) processing of whole mounts. **A–C:** There was a uniform distribution of NPY-IR axons throughout the bladder (a: base; b: middle; c: dome). **D–F:** NPY-IR neurons, commonly in clusters, were found in the detrusor. **G–I:** Numerous para- and peri-vascular NPY-IR axons were associated with all branches of the vasculature tree. **J–L:** NPY-IR axons were found in the suburothelial plexus and became progressively less dense towards the bladder dome (J: base; K: middle; L: dome). **M–O:** The majority of NPY-IR axons in the suburothelial plexus originated from para-vascular axons that branched from the mucosal vascular tree. Numbered arrowheads in (G–I) indicate primary, secondary, tertiary and quaternary vessel branches. Arrowheads in (M–O) indicate para-vascular axons branching off the vascular tree. Box in (N) is magnified in (O). Scale bar = 200 μm in (A) also applies to (B, C, G–I, M, N) and represents 100 μm in o; 50 μm in (D) also applies to (D, F, J–L).

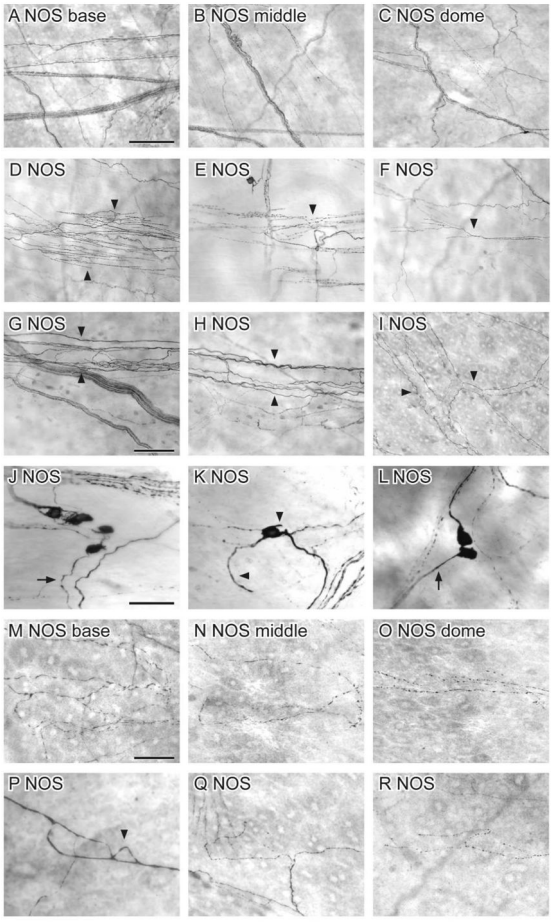

Figure 13.

Distribution of nitric oxide synthase (NOS)-immunoreactivity (IR) in the bladder, viewed using DAB processing of whole mounts. **A–C:** NOS-IR axons showed a uniform distribution throughout the bladder (A: base; B: middle; C: dome). **D–F:** Many specialised NOS-IR nerve endings (arrowheads) were observed throughout the bladder. **G–I:** NOS-IR axons were associated with the vasculature (arrowheads) in the detrusor (G, H) and lamina propria (I). **J–L:** NOS-IR neurons were distributed throughout the bladder and found individually (K) or in small clusters (J, L). The length of their dendrites varied widely between neurons (compare arrrowheads in K). **M–O:** NOS-IR axons were found in the suburothelial plexus and became progressively less dense towards the bladder dome (M: base; N: middle; O: dome). **P**: A NOS-IR closed axonal loop (arrowhead) in the suburothelial plexus. **Q, R:** NOS-IR axon terminals were also observed in the suburothelial plexus; weak to moderate labelling was also present in urothelial cells. Scale bar = 500 μm in A (also applies to B, C); 100 μm in D (also applies to E, F); 50 μm in G (also applies to H, I); 50 μm in J (also applies to K–L); 50 μm in M (also applies to N–R).

Table 1

Primary Antibodies Used for Immunohistochemistry

Antigen	Description of immunogen	Supplier/catalogue number	Dilution
Calcitonin gene-related peptide (CGRP)	GG-conjugated synthetic peptide corresponding to amino acids 23–37 of rat Tyr-CGRP	Biogenesis (now AbD Serotec), goat polyclonal, Cat# 1720-9007, RRID:AB_2290729	1:2000
Calcitonin gene-related peptide (CGRP)	KLH-conjugated rat synthetic peptide	Millipore, rabbit polyclonal Cat# AB5920, RRID:AB_2068655	1:5000
Glial fibrillary acidic protein (GFAP)	GFAP isolated from cow spinal cord	Dako Cat# Z0334, rabbit polyclonal, RRID:AB_10013382	1:1000
Glial cell line-derived neurotrophic factor family receptor α3 (GFRα3)	Recombinant protein corresponding to amino acid sequence Glu34-Arg379 of mouse GFRα3 (Accession # AAB70931)	R&D Systems, goat polyclonal, Cat# AF2645, RRID:AB_2110295	1:300
Neurofilament 200 (NF200)	Neurofilaments of molecular weight 200 kDa in rat spinal cord extract	Sigma-Aldrich, mouse monoclonal, Cat# N0142, RRID:AB_477257	1:4000
Neuropeptide Y (NPY)	BTg-conjugated synthetic porcine NPY	DiaSorin (now ImmunoStar), rabbit polyclonal, Cat# 22940, RRID:AB_572253	1:3000
Neuronal nitric oxide synthase (nNOS)	Recombinant protein corresponding to 195 amino acids from the N-terminus of rat nNos	Zymed (now Invitrogen), rabbit polyclonal, Cat# 61-7000, RRID:AB_2313734	1:500
S100	Purified bovine S100	Millipore, mouse monoclonal, Cat# MAB079-1, RRID:AB_571112	1:500
Smooth muscle actin-α (SMA)	KLH-conjugated synthetic peptide corresponding to 10 amino acids from the N-terminus of SMA	Sigma-Aldrich, mouse monoclonal, Cat# A5228 RRID:AB_262054	1:5000
Tyrosine hydroxylase (TH)	Denatured tyrosine hydroxylase from rat pheaochromocytoma	Millipore, rabbit polyclonal, Cat# AB152, RRID:AB_390204	1:1000
Vimentin (Vim)	Porcine Vim purified from eye lens	Sigma-Aldrich, mouse monoclonal, Cat# V6630, RRID:AB_477627	1:10,000

Table 2

Secondary Antibodies used for Immunohistochemistry

Species	Conjugated	Supplier/catalogue number	Dilution
Anti-goat	Cy3	Jackson ImmunoResearch, donkey polyclonal, Cat# 705-165-147, RRID:AB_2307351	1:1000
Anti-mouse	Alexa 488	Molecular Probes (now Invitrogen), donkey polyclonal, Cat# A21202, RRID:AB_10049285	1:1000
Anti-mouse	Biotin-SP	Vector Laboratories, donkey polyclonal, Cat# BA2000, RRID:AB_2313581	1:1000
Anti-rabbit	Alexa 488	Invitrogen, donkey polyclonal, Cat# A21206, RRID:AB_10049650	1:2000
Anti-rabbit	Biotin-SP	Jackson Laboratories, donkey polyclonal, Cat#711-065-152, RRID:AB_2333077	1:1000
Anti-rabbit	Cy3	Jackson Laboratories, donkey polyclonal, Cat# 711-165-152, RRID:AB_2307443	1:1500
Anti-sheep	Biotin-SP	Jackson Laboratories, donkey polyclonal, Cat#713-065-003, RRID:AB_2333076	1:1000